NASA Technical Memorandum 100068

Vortex Methods for Separated Flows

Philippe R. Spalart

June 1988

National Aeronautics and
Space Administration

NASA Technical Memorandum 100068

Vortex Methods for Separated Flows

Philippe R. Spalart, Ames Research Center, Moffett Field, California

June 1988

National Aeronautics and
Space Administration

Ames Research Center
Moffett Field, California 94035

TABLE OF CONTENTS

ACKNOWLEDGEMENTS

These course notes were written for the Lectures Series on "Computational Fluid Dynamics", March 7-11, 1988, at the von Karman Institute for Fluid Dynamics. The author is grateful to Professors H. Deconinck and J. Essers for their kind invitation. We also thank Mr. K. Shariff and Mr. G. Coleman (NASA Ames Research Center and Stanford University) for many valuable suggestions.

SUMMARY

The numerical solution of the Euler or Navier-Stokes equations by Lagrangian "vortex methods" is discussed. The mathematical background is presented in an elementary fashion and includes the relationship with traditional point-vortex studies, the convergence to smooth solutions of the Euler equations, and the essential differences between two- and three-dimensional cases. The difficulties in extending the method to viscous or compressible flows are explained.

The overlap with the excellent review articles available is kept to a minimum and more emphasis is placed on the author's area of expertise, namely two-dimensional flows around bluff bodies. When solid walls are present, complete mathematical results are not available and one must adopt a more heuristic attitude. The imposition of inviscid and viscous boundary conditions without conformal mappings or image vortices and the creation of vorticity along solid walls are examined in detail. Methods for boundary-layer treatment and the question of the Kutta condition are discussed.

Practical aspects and tips helpful in creating a method that really works are explained. The topics include the robustness of the method and the assessment of accuracy, vortex-core profiles, time-marching schemes, numerical dissipation, and efficient programming. Operation counts for unbounded and periodic flows are given, and two algorithms designed to speed up the calculations are described.

Calculations of flows past streamlined or bluff bodies are used as examples when appropriate. These include curved mixing layers, the starting vortex and the dynamic stall of an airfoil, rotating stall in a two-dimensional cascade, a multi-element airfoil, and an attempt at predicting the drag crisis of a circular cylinder.

1. INTRODUCTION

Vortex methods in general were thoroughly reviewed by Leonard (1980, 1985), and it would be difficult to improve on these articles. In the present notes we intend to cover the basics of vortex methods and then to discuss in more depth two subjects: the interaction with solid walls, and the practical aspects of programming and using vortex methods. These subjects were of less interest to Leonard, but are crucial in engineering applications. Therefore we attempt to present useful and sometimes original material in these areas. We shall also mention some recent contributions, published after Leonard's articles. The sections which contain advanced material and could be omitted for a first reading are indicated by stars.*

1.1. Example: Flow Past a Multi-Element Airfoil

We propose to start by showing a calculation of a separated flow via the vortex method to illustrate its main features and, we hope, render it attractive to the reader. We shall often describe the method by comparison with grid-based (finite-difference or finite-element) methods, since these are more widespread.

In 1986 the Boeing Commercial Airplane Company contacted the author, asking for computations of the flow past an airfoil in landing configuration, with a leading-edge slat and a double-slotted trailing-edge flap. Boeing was especially interested in the variation of the lift with Reynolds number. The configuration was a severe test for numerical methods due to the complex, multiply connected shape and the importance of viscous effects, including separation.

Results were obtained in less than a week. In spite of the many concave and convex sharp corners present, no smoothing or other alteration of the shape was necessary. This illustrates the first advantage of the vortex method: it is grid-free. With a finite-element or especially a finite-difference method the grid generation for such a shape would be difficult and time consuming, and one may have to settle for rather distorted grids which degrade the accuracy. With the vortex method the only precaution taken was to make the spacing between vortices and the time step small enough to accomodate the narrow gaps between elements 2 and 3, and 3 and 4 of the airfoil.

Figure 1 shows the airfoil, the vortices (more accurately, the centers of the vortex blobs), streamlines, and the individual (hollow arrowheads) and overall (filled arrowhead) force vectors at a given time. Observe the recirculating bubble behind the slat, the acceleration of the fluid through the slots, the separation at sharp corners and on the top surface of element 4, and the irregular motion in the wake. The computed forces were in good agreement with experiment. The figure illustrates the Lagrangian character of the method: the solution procedure consists in tracking vortices which move with the fluid, rather than updating quantities at fixed grid points. It also illustrates the second advantage of the method: the vortices carry all the information and are needed only in a narrow region near the body and in the wake. In fact the calculation used just 1300 vortices (roughly the equivalent of a single 36×36 grid). The streamlines were computed only for display purposes; for the purpose of advancing the equations in time, computing the forces, etc.,

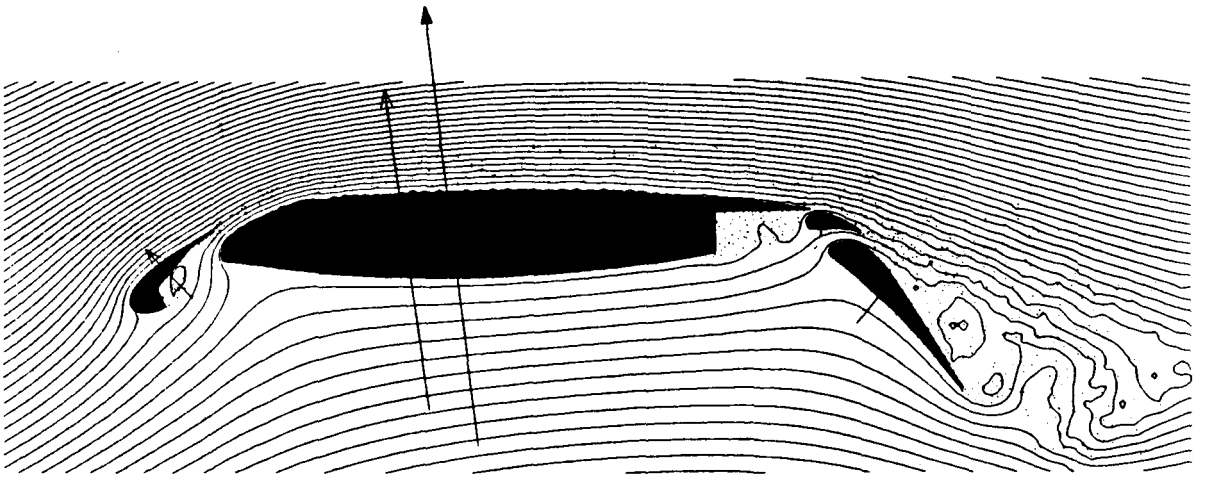

Figure 1. Flow past a multi-element airfoil. $\cdots$ vortices; $\uparrow$ forces; — streamlines

one only needs to compute the velocity of the vortices themselves.

Additional advantages of the method are first that the boundaries of the computed domain are at infinity which removes all of the problems associated with computations in a truncated domain (the effects of the boundary conditions on accuracy and on stability) and second that there is low numerical dispersion. The method can transport flow structures (groups of vortices) at any velocity without deforming them or dissipating them as a grid-based method may do. There is no CFL number. The question of time accuracy will be addressed in much more detail later.

Among the disadvantages are the fact that the flow had to be treated as incompressible, although fairly high local Mach numbers may be reached in the slots even at the landing speed. The calculation also required the storage of a 249×249 full matrix and about 5×10^{11} floating-point operations to establish the flow, starting from rest, and generate a time sample long enough for averaging. Both figures are much larger than what a 36×36 grid calculation would require. Thus, a vortex carries much more information than a grid point, but it is also much more expensive to maintain. This is because all the vortices interact, so that the operation count is of order N^2, where N is the number of vortices. The competing methods often have operation counts of order N or $N\log(N)$.

To answer Boeing's question, a Reynolds number dependence was indeed predicted. As the chord Reynolds number was changed from 2.3×10^6 to 1.2×10^7 with all the other parameters (physical and numerical) exactly the same, the lift coefficient at 8^o incidence increased by about 5%. This was caused by a difference in the boundary-layer behavior on the upper surface of element 4. At the lower Reynolds number, the boundary layer always separated, whereas at the higher Reynolds number it could transition and remain attached part of the time, thus increasing the circulation around element 4 and therefore the overall lift. This Reynolds-number trend was consistent with the common wisdom. Ironically, Boeing subsequently informed the author that experiments had predicted an

opposite trend for this configuration, so that the situation was rather confused. This study demonstrates the power of a well-designed vortex method in dealing with complex geometries, and how challenging and unpredictable Reynolds-number effects can be to numericians, experimentalists, and designers.

1.2. Governing Equations

Complete discussions of these equations can be found in textbooks, e.g., Batchelor (1967). The fundamental equations are the incompressible Navier-Stokes equations,

$$\nabla.\mathbf{U} = 0 \tag{1a}$$

$$\mathbf{U}_t + \mathbf{U}.\nabla\mathbf{U} = -\nabla p + \nu\nabla^2\mathbf{U}. \tag{1b}$$

Here $\mathbf{U}$ is the velocity vector, ∇ is the gradient operator, t is the time, p is the kinematic pressure, and ν is the kinematic viscosity. Bold-face letters like $\mathbf{U}$ denote vector quantities, and the symbol $\equiv$ indicates a definition. Equation (1a) is the continuity equation and (1b) the momentum equation. One obtains the Euler equations by setting $\nu = 0$. The vorticity ω is the curl of the velocity,

$$\omega \equiv \nabla \times \mathbf{U}. \tag{2}$$

In an unbounded domain with the fluid at rest in the far field, one has the "Biot-Savart law", which is the inverse of (2) by a Green's-function approach (when (1a) holds) and explicitly gives the velocity in terms of the vorticity:

$$\mathbf{U}(\mathbf{x}) = \frac{1}{4\pi}\int \frac{\omega(\mathbf{x}') \times (\mathbf{x} - \mathbf{x}')}{|\mathbf{x} - \mathbf{x}'|^3}\, d\mathbf{x}'. \tag{3}$$

This equation only expresses the kinematics of the flow. The integral, taken over the whole two- or three-dimensional (2-D, 3-D) domain, is responsible for the nonlocal interactions between vortices. By taking the curl of (1b) one gets the vorticity equation,

$$\omega_t + \mathbf{U}.\nabla\omega = \omega.\nabla\mathbf{U} + \nu\nabla^2\omega. \tag{4}$$

Notice that the pressure term is eliminated, but that a new term, $\omega.\nabla\mathbf{U}$, appears which is responsible for vorticity stretching and rotation. In this term, $\nabla\mathbf{U}$ can be replaced by its symmetric part $(\nabla\mathbf{U} + \nabla\mathbf{U}^T)/2$ (the deformation tensor), which may be advantageous in some numerical methods (Cantaloube and Huberson, 1984).

The circulation of a velocity field $\mathbf{U}$ along a closed contour is defined by the line integral

$$\Gamma \equiv \oint \mathbf{U}.d\mathbf{l}. \tag{5}$$

This is an extremely useful concept because Kelvin's theorem (Batchelor, 1967, p. 273) shows that in the absence of viscosity, the circulation around a contour that follows the fluid is conserved: $D\Gamma/Dt = 0$.

In 2-D the equations are much simpler. If the flow is in the (x, y) plane the vorticity only has a component in the z direction, $\omega_z \equiv \partial v/\partial x - \partial u/\partial y$ (which we'll denote simply by ω). The Biot-Savart law becomes

$$\mathbf{U}(\mathbf{x}) = \frac{1}{2\pi}\ \mathbf{e}_z \times \int \frac{\mathbf{x} - \mathbf{x}'}{|\mathbf{x} - \mathbf{x}'|^2}\ \omega(\mathbf{x}')\ d\mathbf{x}' \tag{6}$$

with $\mathbf{e}_z$ the unit vector in the z direction. The vorticity equation (4) becomes

$$\omega_t + \mathbf{U}.\nabla\omega = \nu\nabla^2\omega. \tag{7}$$

Note that the rotation/stretching term has disappeared. One can define a scalar stream function ψ by $\mathbf{U} \equiv \mathbf{e}_z \times \nabla\psi$ since $\mathbf{U}$ is divergence-free. Then ψ satisfies a Poisson equation, $\nabla^2\psi = \omega$, and the Biot-Savart law is written

$$\psi(\mathbf{x}) = \frac{1}{2\pi}\int \omega(\mathbf{x}')\log(|\mathbf{x} - \mathbf{x}'|)\ d\mathbf{x}'. \tag{8}$$

1.3. Invariants of the Motion

One important source of confidence in a numerical method is its conservation of at least some of the appropriate integral quantities. In the present context, the most useful form of these invariants is in terms of the vorticity, rather than the velocity. See the discussions by Batchelor (1967, p. 517), Wu and Sankar (1980) or Ting (1983); the arguments rely on integrations by parts but are subtle, because the velocity decays slowly (algebraically) at large distances even when the vorticity decays fast (exponentially) which is the usual situation. In 3-D the important integrals are

$$\int \omega\ d\mathbf{x}, \tag{9}$$

$$\int \mathbf{x}\ \times \omega\ d\mathbf{x}, \tag{10}$$

$$\int \mathbf{x} \times (\mathbf{x} \times \omega)\ d\mathbf{x}, \tag{11}$$

$$\int \frac{\omega(\mathbf{x}).\omega(\mathbf{x}')}{|\mathbf{x} - \mathbf{x}'|}\ d\mathbf{x}\ d\mathbf{x}'. \tag{12}$$

They correspond to total vorticity, linear momentum, angular momentum, and kinetic energy, respectively. We assume that the vorticity decays fast enough in the far field for these integrals to be defined. Note that the total vorticity (9) is trivial unless ω decays very slowly, because if it decays any faster than r^{-3}, one can easily show that this integral is identically zero (use $\nabla.\omega = 0$). In 2-D the corresponding quantities are

$$\int \omega\ d\mathbf{x}, \tag{13}$$

$$-\mathbf{e}_z \times \int \omega \ \mathbf{x} \ d\mathbf{x}, \tag{14}$$

$$\int \omega \ |\mathbf{x}|^2 \ d\mathbf{x}, \tag{15}$$

$$\int \omega(\mathbf{x}).\omega(\mathbf{x}') \ \log(|\mathbf{x} - \mathbf{x}'|) \ d\mathbf{x} \ d\mathbf{x}'. \tag{16}$$

Here, the total vorticity (13) has no reason to be zero.

In unbounded inviscid flows, all these quantities are conserved. In unbounded viscous flows, only total vorticity and linear momentum (9, 10, 13, 14) are conserved. Formulas giving the rate of viscous decay of angular momentum and kinetic energy can be found (e.g., Ting, 1983). When there is a solid body in the fluid it can alter any of the integrals (9-16). However, the variation of (9) and (13) (with the integrals restricted to the fluid region) is known once the motion of the body is (Wu and Sankar, 1980).

The invariants are often invoked when constructing or evaluating methods, but the actual importance of exactly conserving quantities such as (9-16) in a numerical method is a matter of debate. The invariants are integrals over the whole domain, and contain no information about the details of the solution. Many successful methods violate some of the invariants, especially once time-integration errors are included, and one can construct methods that conserve the invariants but are not very good or even are inconsistent. The common argument that energy conservation prevents the calculation from "blowing up" is rather technical, and in any case does not directly apply to vortex methods.

The following intuitive argument seems more relevant. The conservation of an invariant means that over the whole domain the local errors exactly cancel each other in some measure (e.g., $|\mathbf{x}^2|d\mathbf{x}$ for (15)). From a statistical point of view, it is then reasonable to expect that over an intermediate domain, large enough to contain many vortices or grid points, the local errors tend to cancel each other instead of accumulating. One then expects much better accuracy on intermediate scales than on small scales. This is probably true in many vortex calculations, especially complex ones such as in figure 1. One can tolerate significant errors in the irregular small-scale motion, as long as they do not affect the quantities of interest such as the forces and moments on the bodies.

*1.4. Constraints on Vector Fields**

Vortex methods and related methods focus on derivatives (or combinations of derivatives) of the primary variables. Using a collection of computational elements (e.g., vortices) one can represent an arbitrary vector field. This can become a liability, because many of the vector fields involved are *not* arbitrary; they satisfy constraints. For instance, if the vector $\mathbf{A}$ is the gradient of a scalar, say $\mathbf{A} \equiv \nabla\phi$, then $\nabla \times \mathbf{A} = 0$. Now if one represents the components of $\mathbf{A}$ separately with two collections of computational elements there will in general be an inconsistency because $\partial A_x/\partial y$ may not be equal to $\partial A_y/\partial x$, and if they do differ there is no scalar ϕ such that $\partial\phi/\partial x = A_x$ and $\partial\phi/\partial y = A_y$. For instance Anderson (1985a) proposed a Lagrangian method for the transport of a gradient and avoided this question by solving a Poisson equation for ϕ: $\nabla^2\phi = \partial A_x/\partial x + \partial A_y/\partial y$, instead of the original equations. For the vorticity, the constraint is that it should be divergence-free:

$\nabla.\omega = 0$. As we shall see this also caused problems, and again some methods had recourse to a Poisson equation ($\nabla^2 \mathbf{U} = -\nabla \times \omega$).

A more direct response to the question of the constraints is to "build them" into the discretization. For instance the Contour Dynamics method (Zabusky, Hughes, and Roberts, 1979) can be regarded as based on computational elements that "carry" $\nabla\omega$, the gradient of the 2-D (scalar) vorticity, but the elements are automatically arranged on chains so that the vector field that purports to be $\nabla\omega$ is indeed curl-free. The equivalent for the vorticity is the filament method, in 3-D. Such "chained" methods are inconvenient in terms of bookkeeping (note how the Contour Dynamics method was never applied to more than a few chains), but are more attractive intuitively. This will be discussed again in the context of the 3-D methods.

2. POINT-VORTEX METHODS

2.1. Basics

Point-vortex studies have a long history. Interest in them is justified by the fact that the dynamics of point vortices provide exact albeit singular solutions of the incompressible Euler equations in 2-D. Assuming one can perform the time integration either analytically or numerically with high accuracy, one can generate nontrivial Euler solutions with a small computational cost and very little memory.

Consider a collection of N vortices at positions $\mathbf{x}_j$, $j = 1, N$, with circulations Γ_j. The vorticity distribution is

$$\omega(\mathbf{x}) = \sum_{j=1}^{N} \Gamma_j \, \delta(\mathbf{x} - \mathbf{x}_j) \tag{17}$$

where δ is the 2-D Dirac distribution (δ is infinite at the origin, 0 elsewhere, and its integral is 1). Thus we have a collection of "spikes" of vorticity. Inserting (17) into (6) we get a sum:

$$\mathbf{U}(\mathbf{x}) = \frac{1}{2\pi} \, \mathbf{e}_z \times \sum_{k=1}^{N} \Gamma_k \frac{\mathbf{x} - \mathbf{x}_k}{|\mathbf{x} - \mathbf{x}_k|^2}. \tag{18}$$

As an exercise one can verify that the velocity field given by (18) is divergence-free, is irrotational except at the points $\mathbf{x}_k$, and has a circulation Γ_k around any contour enclosing only the k^{th} vortex.

The other ingredient, which expresses the dynamics, is Kelvin's theorem. If we make each vortex follow the fluid and imagine a small contour around it we get the result that the circulation Γ_j of each vortex is conserved. Therefore,

$$\frac{d\Gamma_j}{dt} = 0, \tag{19}$$

$$\frac{d\mathbf{x}_j}{dt} = \mathbf{U}(\mathbf{x}_j, t). \tag{20}$$

The formulation is now complete. The unknowns are $\mathbf{x}_j$ and Γ_j, $j = 1, N$. The time evolution is given by (19) and (20), with (18) giving $\mathbf{U}$ in (20). Note that (18) is singular when $\mathbf{x}_j = \mathbf{x}_k$; this contribution is simply omitted from the sum. In other words there is no self-induced velocity for the vortex. The circulations are constant, and the only task is to move the vortices with the fluid.

An early example of point-vortex studies is Rosenhead's (1931). As an exercise one can program the equations (using one's favorite explicit time-integration scheme for now) for two vortices with various circulations of the same sign or of opposite signs. The vortices should orbit around their centroid $(\Gamma_1\mathbf{x}_1 + \Gamma_2\mathbf{x}_2)/(\Gamma_1 + \Gamma_2)$ unless their circulations are exactly opposite, in which case the pair moves in a straight line.

Even though (17) looks like a simple linear superposition of solutions, it is not, because the vortices interact through (18). This is how the nonlinearity of the Euler equations enters the vortex equations. Note also that the equations (18,20) can be derived from the

Hamiltonian $H \equiv -\sum \Gamma_j \Gamma_k \log|\mathbf{x}_j - \mathbf{x}_k|/4\pi$ with $\Gamma_j x_j$ and y_j as the canonically conjugate coordinates and momenta (Aref, 1983). H corresponds to (16) with the self-energy of each vortex (which would be infinite) omitted; in that sense it is the "interaction energy". Naturally, H is conserved by the dynamical equations.

To be rigorous, the point-vortex method can only represent very special vorticity distributions, namely superpositions of Dirac distributions as in (17). These Dirac distributions are singular, and so is the velocity field they induce: it tends to ∞ like $1/|\mathbf{x} - \mathbf{x}_k|$ as $\mathbf{x}$ approaches $\mathbf{x}_k$. Such flows are not realistic in the sense that they have unbounded velocities, infinite kinetic energy, etc. However, if one considers flows with small but nonsingular vortices the point-vortex method is still useful as we show below.

An example of a realistic thin vortex is the "spreading line vortex" which is a classical exact solution of the 2-D Navier-Stokes equations (Batchelor, 1967, p. 204). The vorticity is given by

$$\omega(\mathbf{x}, t) = \frac{\Gamma}{4\pi\nu t} \exp\Big(-\frac{|\mathbf{x}|^2}{4\nu t}\Big), \tag{21}$$

the vortex being centered at the origin ($\mathbf{x}_j = 0$). As the product νt tends to 0, (21) approaches the Dirac distribution (17). The velocity induced by this vorticity is

$$\mathbf{U}(\mathbf{x}, t) = \frac{\Gamma}{2\pi}\, \mathbf{e}_z \times \frac{\mathbf{x}}{|\mathbf{x}|^2}\left(1 - \exp\Big(-\frac{|\mathbf{x}|^2}{4\nu t}\Big)\right). \tag{22}$$

As νt tends to 0 this velocity tends, point by point, to the one given by (18). Thus if the distance between vortices is large compared with their radius ($\sqrt{\nu t}$) the equations (18, 19, 20) will not be affected. More generally, if we have small patches of vorticity (not necessarily of the type of (21)) of extent ϵ much smaller than the distance d between patches the interaction of the vortices through (18) will not be affected. The patches also have internal dynamics; they deform, and spread if viscosity is present. However it can be shown that the centroid of the vorticity in the patch is not affected by the internal dynamics (convective or viscous) (see (14)). Therefore if $\mathbf{x}_j$ represents the centroid of the patch, the self-induced velocity is still exactly zero.

The conclusion is that as the ratio ϵ/d tends to zero the motion of the patches tends to that of point vortices. This was shown rigorously by Marchioro and Pulvirenti (1983) for short times, and it is reasonable to expect that it holds for all times, except maybe for some very special initial conditions. For the gravitational law and well-separated planets the analog is the familiar point-mass approximation. Saffman and Meiron (1986) present a different argument, showing that point vortices provide a weak solution of the vorticity equation (7) with $\nu = 0$ (although according to C. Greengard and Thomann (1988) this is controversial, and depends on one's interpretation of how the Dirac distribution acts on a singular function such as (18)). Thus the point-vortex method is not strictly limited to vorticity fields of the type of (17); it is also a good approximation for the motion of small, well-separated patches of vorticity. This is still too restrictive for most practical applications. Consequently the recent work with point vortices tends to focus on mathematical issues like the Hamiltonian character of the equations, the existence of steady configurations, integrable and chaotic motion (Aref, 1983), the statistical properties, and mixing of the fluid surrounding the vortices. A more elaborate model for well-separated

patches is the "moment model" of Melander, Zabusky, and Styczek (1986), which includes an approximation of the inviscid internal dynamics.

*2.2. Difficulties with Vortex Sheets**

Given sufficient computing power it is natural to use more and more vortices to obtain a finer and finer description of a given vorticity distribution, just like one refines a grid. This idea was first applied to vortex sheets. Such flows are not as strongly singular as point vortices: the vorticity is still singular but only like a 1-D Dirac distribution, the velocity is discontinuous but finite. In fact Rosenhead's work was aimed at a vortex sheet, but he did the computations by hand and could not use a large number of vortices. When this became possible, the outcome was a disappointment: smooth sheets could not be maintained, and the vortices rapidly started moving chaotically (Birkhoff, 1962). The time integration was accurate, and the situation did not improve as more vortices were used (Moore, 1979). Ostensibly, the method was not converging.

The consensus now is that the wrinkling of the sheets discretized with point vortices was not just a numerical phenomenon, because the vortex-sheet problem is not well posed: in general the exact solution does not remain smooth even if the initial condition is. This is so because waves of all scales are unstable, and the shortest waves grow the fastest. Krasny (1986) and other researchers have shown that a periodic vortex sheet disturbed by a single sine wave remains smooth for a finite time, and then develops a singularity (infinite curvature). Krasny explains that if the initial condition is analytic the amplitude of the short waves is exponentially small, so that even though they grow very fast they do not contaminate the whole solution until some finite critical time t_c. Krasny showed that the point-vortex method gave a good solution up to time t_c, but only if round-off errors were reduced to a low enough level. He suggested using higher-precision arithmetic, and also proposed a filtering technique which is very powerful, but should be used with exquisite care.

*2.3. Application to Smooth Euler Solutions**

The point-vortex method is not considered a viable numerical method to converge to smooth solutions of the 2-D Euler equations. However, the reason is not that it would fail in a blatant way, as it seemed to do with vortex sheets. The main reason the point-vortex method is out of favor is that convergence proofs have been given for vortex-blob methods (§**3**) and demand that the blobs overlap, and overlap more and more as they become denser. This is incompatible with point vortices. There is the question of what measure of the error one is using. If one takes the velocity or vorticity fields, there is no way the point-vortex solution could converge in any of the familiar norms, e.g., L_∞, since it is not even bounded. On the other hand if one only considers the trajectory of the vortices and their initial arrangement is regular, they behave well at least for some time, which implies that the global measures like the moments of the vorticity and the Hamiltonian (13-16) behave well too. It may be that the trajectories (and even the velocity field if one takes an "exotic" norm like a Sobolev norm with a negative index) converge to the exact ones at least up to some critical time. This is just a conjecture.

3. VORTEX-BLOB METHODS

3.1. Motivation and Basics

Initially a strong motivation to switch from point vortices to nonsingular (or less-singular) elements than was the failure of the method on vortex sheets (Chorin and Bernard, 1973, Kuwahara and Takami, 1973). Now, the emphasis is on smooth Euler solutions, for which the blob methods have been shown to converge, even with high orders of accuracy (Hald, 1979, Beale and Majda, 1982). We present the method in 2-D. In a vortex-blob method the Dirac distributions δ in (17) are replaced by bounded functions δ_σ:

$$\omega(\mathbf{x}) = \sum_{j=1}^{N} \Gamma_j \, \delta_\sigma(\mathbf{x} - \mathbf{x}_j). \tag{23}$$

The δ_σ function has an integral of 1, and the length scale σ (the "core radius") is a measure of the spread of δ_σ. In almost all cases, δ_σ is radially symmetric and its shape is independent of σ, i.e.,

$$\delta_\sigma(\mathbf{x} - \mathbf{x}_j) \equiv \frac{1}{\sigma^2} \, f\left(\frac{|\mathbf{x} - \mathbf{x}_j|}{\sigma}\right) \tag{24}$$

for some nondimensional function f, usually bell-shaped, and satisfying

$$2\pi \int_0^\infty r f(r) dr = 1. \tag{25}$$

One now has a "realistic" velocity field, bounded and with locally finite kinetic energy. The function f is small away from the origin, and as $\sigma \to 0$, the blobs resemble point vortices. The Gaussian, as in (21), is a possible choice but may not be the most judicious in terms of computational speed. Equation (18) becomes

$$\mathbf{U}(\mathbf{x}) = \frac{1}{2\pi} \, \mathbf{e}_z \times \sum_{k=1}^{N} \Gamma_k \frac{\mathbf{x} - \mathbf{x}_k}{|\mathbf{x} - \mathbf{x}_k|^2} F\left(\frac{|\mathbf{x} - \mathbf{x}_k|}{\sigma}\right) \tag{26}$$

where F is defined by

$$F(r) \equiv 2\pi \int_0^r r' f(r') dr'. \tag{27}$$

Figure 2 gives an example of the velocity given by (26, 27), compared with the point-vortex velocity (18). They agree except for $|x|/\sigma$ of the order of 1 or less, and the blob-induced velocity is smooth at the origin. Finally the stream function is given by

$$\psi(\mathbf{x}) = \frac{1}{2\pi} \sum_{k=1}^{N} \Gamma_k \, \tilde{F}\left(\frac{|\mathbf{x} - \mathbf{x}_k|}{\sigma}\right) \tag{28}$$

with $\tilde{F}$ defined by

$$\tilde{F}(r) \equiv \int_0^r \frac{F(r')}{r'} \, dr'. \tag{29}$$

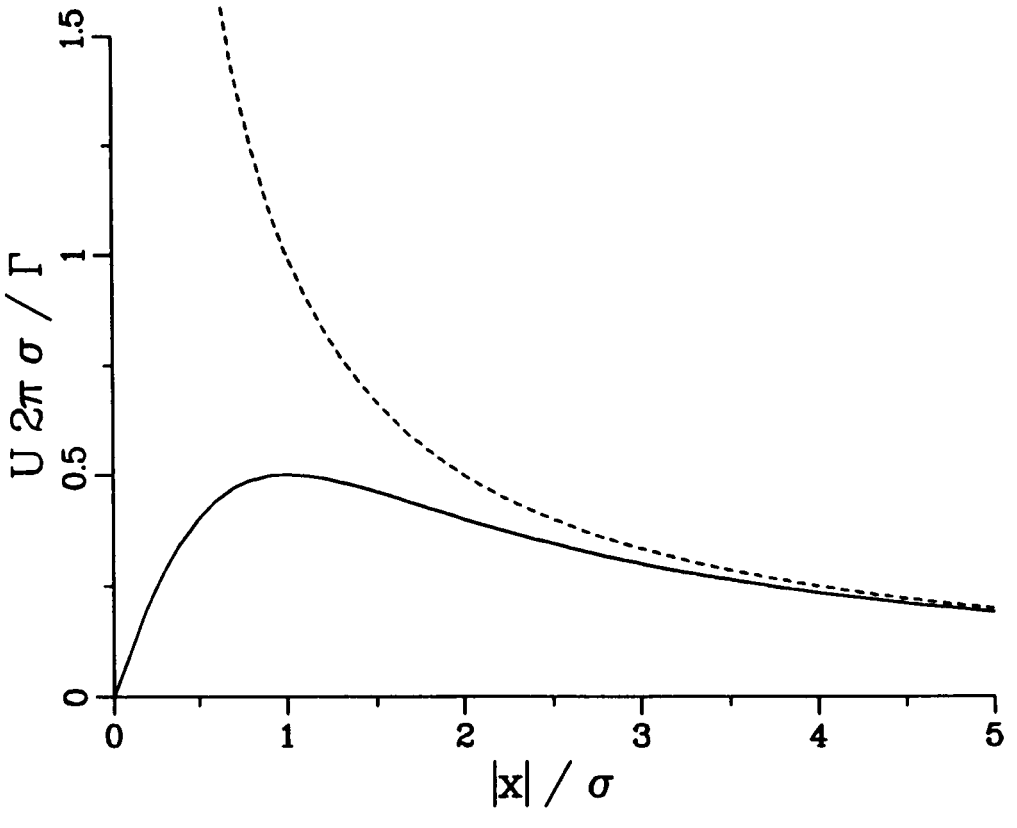

Figure 2. Azimuthal velocity induced by vortices. — vortex blob; - - - point vortex

Equation (19) is unchanged; circulation is conserved. In most methods (20) is also unchanged, i.e., the blob moves with the velocity at its center $\mathbf{x}_j$. Leonard (1980) discusses the use of the velocity averaged over the blob (weighted by δ_σ) instead of the velocity at the center. In that case, (27) does not hold and the relation between f and F is slightly more complex; the alteration of the velocity is $O(\sigma^2)$. Averaging the velocity is sensible since the most meaningful interpretation of $\mathbf{x}_j$ is as the centroid of a small vortex patch (§*2.1*). Leonard also shows that the kinetic energy of the flow (16) is conserved only with the weighted scheme. On the other hand, this energy strongly depends on the function f, which has little physical meaning, and given a function F one can always define a Hamiltonian which approximates the kinetic energy, and will be conserved. The weighted scheme has not received much use.

One could consider using a different core radius σ_j for each vortex; however this is ill-advised because it prevents the method from conserving even the most basic invariants, e.g., the linear momentum (14) (Leonard, 1980). One can of course symmetrize the interaction by taking an average of σ_j and σ_k, which restores the conservation of (14), but this is arbitrary and seems inconsistent with the concept that the exact value of σ_j is important. A much better response to the objection that (14) is not conserved would be to use Leonard's

weighted scheme. Still, the consensus is that the calculations are, and should be, quite insensitive to the function f and the value of σ. The basic method defined by (19, 20, 26) with uniform σ (independent of j or t) is by far the most used.

3.2. Convergence in Theory

The accuracy and convergence have been discussed by Hald (1979), Leonard (1980), and Beale and Majda (1982), among others. Leonard focused on the consistency of the method whereas Hald, and Beale and Majda obtained complete convergence proofs including stability. Both approaches produced "moment conditions" which indicate the order of accuracy of the method according to whether some integrals of the function f equal 0.

Beale and Majda split the error in the velocity field at some time t into two components, one due to the inexact position of the vortex centers (compared with the motion of the points in the exact solution), and the other due to the discretization of the velocity by (26). The two components naturally interact as t increases. Leonard examined the local error due to the fact that the whole blob is made to move at the same velocity, whereas in reality the fluid region that coincides with it is strained. He did not emphasize the error due to the initial discretization.

The mathematical papers all show that convergence is obtained when $N \to \infty$, $h \to 0$, and $\sigma \to 0$, but σ not as fast as h (i.e., $\sigma/h \to \infty$). This last condition was unexpected (Leonard, 1980); it means that the vortices must become closely spaced, but also overlap more and more for the method to converge. Empirical tests by Nakamura *et al.* (1982) and Perlman (1985) fully confirm the need for the increased overlap. Hald and Beale and Majda suggest simple laws like $\sigma = Ch^q$ with C some constant and the power q less than 1. The studies by Hald, Leonard, and Beale and Majda all show that the error is proportional to some power of σ, not h. For instance with a Gaussian core function f the error is of order σ^2.

The initialization of the vortices is more involved than one might expect, even in the simple case of an unbounded domain. Suppose one has an initial vorticity field ω_0. One lays a grid of cells of size h over the domain. One procedure is to place a vortex at the center of each cell, and to give it the circulation within that cell (the integral of ω_0 over the cell). The vorticity centroid would then be preferable to the geometric center of the cell. Another is to give it the value of ω_0 at the center, multiplied by h^2. The first procedure is more intuitive and is preferable if ω_0 is not smooth; the second one is formally more accurate and is recommended if one is seeking better than second-order accuracy and ω_0 is very smooth. A third procedure is to require that the vorticity given by (23) equal ω_0, either at the grid points or at a denser set of points with a least-squares algorithm (Nakamura *et al.*, 1982). This results in a matrix equation for the Γ_j's. This idea is attractive, but the implementation can be awkward, and the matrix is very ill-conditioned if σ/h is large.

3.3. Convergence in Practice

Convergence has been tested and observed only for unbounded flows (wall-bounded

flows are discussed in §*9.6*). Many papers contain some useful information about the behavior of the method (Nakamura *et al.*, 1982; Beale and Majda, 1985), but Perlman's 1985 study is the most complete. She chose some simple, smooth, radially symmetric Euler solutions and systematically computed the errors in actual calculations, including the various components introduced by Beale and Majda (1982). She found that for smooth ω_0 the method did converge, with the expected order of accuracy. For less-smooth ω_0 the higher-order cores (ones which satisfy more moment conditions) did not provide any advantage. Values of the power q close to 1 (little overlap of the cores) made the calculation lose its accuracy in a shorter time. The disorganization of the vortices, compared with their regular initial arrangement, was largely responsible for the loss of accuracy.

The question of disorganization is very relevant, because in practice the vortices always look disorganized, see figure 1. In all flows of interest, the product of the time and the velocity gradients (strain rate, vorticity) is large, so that the fluid gets highly distorted. The advantage of the vortex method over the few grid-based Lagrangian methods that have been tried is precisely that it can tolerate this distortion. However, its order of accuracy seems to drop to lower values. Quite probably, most vortex calculations produce results that are quantitatively accurate (especially the global quantities, e.g., forces and moments) but are far out of the range where the theoretical error estimates apply (§*1.3*, *9.6*). This is at the same time a weakness, and a strength.

4. THREE-DIMENSIONAL FLOWS*

*4.1. Essential Differences with Two-Dimensional Flows**

There are two differences: the constraint on the vorticity to be divergence-free is not trivial, and infinitely thin vortices are not a viable approximation. The constraints were discussed in §*1.4*. In 3-D an arbitrary collection of Dirac functions as in (17), or of their smoothed counterparts as in (23), does not satisfy $\nabla.\omega = 0$ and therefore cannot represent a vorticity field. This difficulty has been addressed in two ways. One is to chain the vortex elements together to form filaments or nets, which automatically imposes the constraint. The other is to ignore the constraint at the level of the discretization and to rely on the accuracy of the method: as the method converges the constraint is better and better satisfied, as is the other equation (4). The first approach produced the filament and segment methods, while the second produced the "monopole" methods.

The second difference is also a major difficulty. The velocity of a thin vortex filament of circulation Γ, radius of curvature R, core radius a, and binormal vector $\mathbf{b}$ is approximately given by

$$\mathbf{U} \approx \frac{\Gamma}{4\pi R} \log\left(\frac{R}{a}\right)\mathbf{b} \tag{30}$$

(see Batchelor, 1967, p. 523). Thus filaments with curvature have a self-induction, and moreover it is not well behaved in the limit of an infinitely thin filament ($a/R \to 0$). The next term in the approximation, after (30), strongly depends on the shape of the vorticity distribution, e.g., a "top hat" or a Gaussian as in viscous flows (21). This behavior of the self-induced velocity has motivated a number of studies based on the Local Induction Approximation (LIA) (Hama, 1962). Consider a smooth vortex with circulation Γ and global length scale L, and assume that $a/L \to 0$. If one integrates from time 0 to T and the product $T\ \Gamma \log(L/a)/L^2$ is kept constant, the motion of the vortex tends to a finite limit as $a/L \to 0$, given by (30). Observe that (30) depends only on the local characteristics of the vortex.

The LIA is reminiscent of the 2-D point-vortex approximation since it describes the motion in the limit of very thin vortices, but is in fact almost the opposite since the internal dynamics, which were negligible in 2-D, now control everything. Also, two distinct filaments do not interact at all, and different parts of the same filament interact weakly through the derivatives that enter the definition of the tangent, the binormal, and the radius of curvature. The LIA became especially popular when Hasimoto (1972) showed that it could support solitons. However in practice it is not easy to justify the value of a or to decide whether a should vary in space or time. The restriction $a << L$ is also unrealistic in any situation with viscous or turbulent stresses. At this point this approximation has given excellent results in a few specific cases (Leonard, 1985), but it is not regarded as a numerical method adapted to the solution of practical problems.

*4.2. Filament Methods**

Filament methods have been introduced and refined by Leonard and his co-workers over

the years (Leonard, 1985). Since vorticity is naturally arranged on closed lines Leonard chooses a discretization based on vortex filaments each with a constant circulation Γ_j. The filaments then induce a velocity field on each other and on themselves, and their motion is computed. The self-induced velocity requires special care because the Biot-Savart kernel, equation (3), is strongly singular and many different regularizations have been tried. The method is in a state of flux, because the regularization that has been used up to now is accurate for long waves (it agrees with (30)) but is not satisfactory for short waves on the filament, often resulting in a spurious instability (Leonard, 1985). Recent work by Winckelmans and Leonard (1987) focuses on a solution to this problem which actually borrows a term from the LIA and adds it to the usual regularized contribution.

Leonard's method is by far the most used in 3-D (Leonard, 1980, 1985, Ashurst, 1983, Ashurst and Meiburg, 1985, Nakamura, Leonard, and Spalart, 1986). See also the closely-related 3-D vortex-in-cell method of Couët, Buneman, and Leonard (1981). With proper care this method can be applied to a variety of vorticity-dominated flows. Some involve isolated filaments, in which case the core parameters have a strong influence on the solution; others involve "bundles" of numerical filaments to describe a physical vortex, which makes the calculation much more expensive but less sensitive to the parameters. A systematic application to flows past solid bodies, with boundary layers, separation, and so on, still has to be made.

*4.3. Segment Methods**

Chorin (1980, 1982) proposed a method in which chains of vortex elements can also be identified, but they are treated totally separately in terms of the velocity they induce, and the simplest and least computationally expensive regularization of the kernel is used (the velocity is corrected within a sphere centered on the mid-point of the segment). Chorin does not require a single chain to behave like a physical vortex, and relies on bundles or clouds of elements to obtain the correct behavior (e.g., (30)). Compared with filament methods this method is somewhat cheaper computationally and offers easier bookkeeping. In fact, one could generalize the pattern of elements from a bundle of lines to a "net". One would keep track of a set of nodes, which get moved in time following the fluid. There would also be a set of segments, each with a circulation, a starting node and an end node. Any number of segments could start from, or end on, a single node provided that their circulations (taken with the appropriate sign) add up to zero. With such a method it would be much easier to merge nodes to control their number if needed (*§9.3*).

Chorin (1982) used his method to compute the evolution of a disturbed vortex in a periodic box, with emphasis on the question of singularities in the 3-D Euler equations and the fractal character of the support of vorticity in turbulent flow. He also studied boundary-layer transition (Chorin, 1980).

*4.4. Monopole Methods**

A number of 3-D methods have been proposed in which the computational elements are totally disconnected instead of being arranged in filaments or nets (Rehbach, 1977;

Saffman, 1980; Beale and Majda, 1982; Novikov, 1983; C. Greengard, 1984; Cantaloube and Huberson, 1984; Anderson and C. Greengard, 1985; Mosher, 1985). The elements are sometimes called "vortex monopoles" or "vortons." In such methods the rotation and stretching of vorticity by the $\omega.\nabla\mathbf{U}$ term is explicitly computed instead of being a by-product of the relative motion of the points that describe the filament. The methods differ primarily in the way this term is computed.

The attractive features of such methods are: simplicity and computational convenience, possibly easier mathematical analysis, and the freedom for the elements to rearrange themselves so that the topology of the vortex lines changes (the "reconnection process"). The objection was raised early on (by the author and certainly by many others) that in such a method the vorticity field carried by the computational elements may not be divergence-free, which is unnatural.

Suppose one has a set of elements which carry vorticity in 3-D space. Call ω_a the vector field formed by adding the vorticity of all the elements, as in (17) or (23) but with vector values. The subscript "a" stands for "apparent", as will become clear. The procedure is to apply the Biot-Savart law (3) to ω_a to obtain the velocity field $\mathbf{U}$. Let us define the "true" vorticity field ω_t by $\omega_t \equiv \nabla \times \mathbf{U}$. Clearly the divergence of ω_t is 0, since it is the curl of some vector field. If the divergence of the apparent vorticity is nonzero, it cannot be equal to the true vorticity: $\omega_a \neq \omega_t$. More precisely, ω_t is the projection of ω_a onto the space of divergence-free vector fields (this is so because the Biot-Savart law actually solves the Poisson equation $\nabla^2\mathbf{U} = -\nabla \times \omega_a$, so that the only link between ω_a and ω_t is that they have the same curl).

Graphically, what this means is that when the "vortex lines" of ω_a terminate within the domain (i.e., $\nabla.\omega_a \neq 0$) the vortex lines of ω_t correct this by connecting to another element, or the opposite end of the same element, in as smooth a fashion as possible. Thus the small region in which $\omega_a \neq 0$ is surrounded by a much larger "halo" in which $\omega_t \neq 0$. This is disturbing, because one applies the vorticity transport equation (including the vortex-stretching and rotation term, etc.) to ω_a, not to ω_t. Thus if there is rotation locally where ω_a is located, the whole halo of ω_t rotates too, which is just not correct.

If the visualization of a monopole calculation shows that the elements are scrambled and some of the vortex lines of ω_a terminate within the domain, then ω_a and ω_t must be strongly different, the calculation is unreliable, and it should be terminated. Monopole methods are unlikely to be "robust" in the sense of allowing safe integration to large times. Rehbach (1977) reports serious problems far downstream of his wing and had to artificially reduce the strength of the vortex elements in that region to obtain a stable solution.

Saffman and Meiron's (1986) study is quite critical of vorton methods. They showed that, in general, a system of vortons is not a weak solution of (4) and does not even conserve the integrated vorticity or momentum, given by (9) and (10) (see also Leonard, 1985); they also comment on the central role of the nonzero divergence of ω_a. Nonconservation of integrated vorticity is not too serious, because it is the integral of ω_a which is not conserved (ω_t always integrates to 0, assuming fast enough decay at large distances). On the other hand, nonconservation of momentum is a serious flaw (*§1.3*).

The most popular application of monopole methods has been to the reconnection process (C. Greengard, 1984; Mosher, 1985), which filament methods are unable to model without

outside intervention. Rehbach (1977) also studied the flow past sharp-edged 3-D wings, and Cantaloube and Huberson (1984) studied propellers and rotors. Only Greengard had a mathematical convergence proof for his method and attempted (with some degree of success) to demonstrate the convergence in actual calculations. The 3-D problem is probably the most open and challenging in the field of vortex methods.

5. EXTENSION TO VISCOUS AND COMPRESSIBLE FLOWS

5.1. Viscous Flows

The original Navier-Stokes equations express local interactions between neighboring points, through the spatial derivatives. In contrast, vortices interact at any distance through the Biot-Savart law and do not recognize their neighbors. The unfortunate consequence is that while we were able to formulate one set of equations, the Euler equations, very elegantly the necessary spatial derivatives are not available to add any other terms, for instance the viscous terms, in a straightforward manner. One needs to alter (19), (20), or (23).

One obvious idea is to use the exact viscous solution (21) to make vortex blobs, at least in 2-D. The blobs then spread in time like $\sqrt{\nu t}$. Equations (19) and (20) are retained. This method is attractive, but inconsistent. In a vortex-blob method, to obtain convergence of the transport process one needs to let the core size σ tend to 0 (see §*3.2*). If σ is made proportional to $\sqrt{\nu t}$, the user can't control it any more, and the core-deformation error cannot be made to vanish. Thus the method "mimics" viscosity, but damages the inviscid process. C. Greengard (1985) actually proved that the method solves "the wrong equation": the vorticity is "correctly diffused, but incorrectly convected, even in the limit of infinitely many vortices".

The most used treatment of viscosity is the random-walk algorithm (Chorin, 1973). Chorin adds a random component of appropriate magnitude (proportional to $\sqrt{\nu \Delta t}$) to the position of each vortex at each time step. In the average, with a large number of vortices, this introduces the desired diffusion. When solid bodies are present there is also a creation of new vortices along the wall at each step to account for the flux of vorticity out of the wall. This approach is very simple, consistent, and partial proofs of convergence are starting to appear (Hald, 1984, Goodman, 1987). On the other hand it seems inefficient to carefully track a vortex if it contains only such a small amount of information (since it takes many vortices for the laws of statistics to turn the random walk process into a meaningful macroscopic diffusion). Milinazzo and Saffman (1977) created a controversy by testing the method and showing very slow convergence to a simple exact solution; the error was of the order of $N^{-1/2}$, with N the number of vortices. There are some questions about which measure of the error is most meaningful with the random vortex method, but the consensus seems to be that slow convergence is observed notably near boundaries (Chorin, 1980), and the $O(N^{-1/2})$ estimate was confirmed by Roberts (1985).

Probably the most convincing application with random walk was the study by Ghoniem and Gagnon (1987). They succeeded in simulating the flow over a backward-facing step in the laminar range, up to Reynolds number 229, using about 1000 vortices. In this flow viscous stresses control the flow even away from the wall, so the agreement with experiments and other calculations is very encouraging. On the other hand, in the author's estimation results of the same quality could be obtained with a grid-based method with much less computational expense, and the competitiveness of the random-walk method in terms of computational speed is not excellent. This led the present author to choose a less ambitious approach, wherein the viscous effects are totally neglected away from the wall,

and are included only in a relatively crude manner in the boundary layers. This approach is clearly not universal, but with careful implementation and high enough Reynolds numbers it has been justified by the results obtained on a number of cases.

Two other possibilities for a viscous method should be mentioned. One could be called the "exploding vortex" method: at each step each vortex would be split into a few vortices with a spread again proportional to $\sqrt{\nu \Delta t}$. This method leads to a rapid proliferation of vortices, and therefore is extremely expensive and impractical. Finally, there is the idea of transferring circulation between blobs at each time step in an appropriate manner to represent the diffusion (G. Winckelmans, personal communication, 1987, after work by Cottet and Raviart's group in France). Thus, (19) is modified. There is no core spreading, so the convergence of the inviscid part of the dynamics is not jeopardized. Circulation is conserved, but the vorticity centroid apparently is not (one could modify (20) to compensate). The method needs to have some "dormant" vortices with zero circulation in any region that may become vortical at later times, and the vortices must be closely packed, only a distance of order $\sqrt{\nu \Delta t}$ apart. In grid-based methods the spacing between points is typically of the order of $\sqrt{\nu T}$ (where T is a global time scale), which is much larger than $\sqrt{\nu \Delta t}$.

The profusion of candidates for the viscous treatment (we even omitted a few that showed very little promise) reflects the intense need for such an addition, as well as the lack of a truly satisfactory solution to this date.

*5.2. Compressible Flows**

Most flows of interest are at least slightly compressible, and the capability to treat such flows with a vortex method would be very valuable. Furthermore one of the key ingredients of the method, Kelvin's theorem of conservation of circulation, still applies to barotropic compressible flows. Shocks and other sources of vorticity invalidate the theorem; this creation of vorticity could in principle be computed, but this has not been attempted yet. Let us restrict the discussion to shock-free flows. Then (19) and (20) apply.

The equation that does not apply any more is (18). The velocity now also depends on the dilatation rate $(u_x + v_y)$, which is nonzero. One possible approach is to include this quantity in the description, and have a number of sources in the flow just like there are vortices. The obstacle here is that the evolution equation for the dilatation rate is far from being as simple as that for vorticity. Furthermore the dilatation rate, unlike the vorticity, is not normally confined to a small region. Thus one of the main advantages of the vortex method is lost. These two obstacles seem to have prevented any sustained attempt using this approach. The author is only aware of some work along these lines by Professor J. C. Wu, using a finite-difference method (personal communication, 1983).

Another approach is to consider flows at low Mach numbers and to approximate the dilatation rate. One would then obtain an expansion in terms of the Mach number, similar to the well-known and successful Prandtl-Glauert approximation. This was attempted by Deffenbaugh and Shivananda (1980). They obtained a Poisson equation for the first correction, of the order the Mach number squared, and used a finite-difference method to solve it. It is not clear to the author that the procedure was consistent, because time

derivatives were found both on the left- and right-hand side of the equations. Indeed the numerical solutions were unstable in time, and Deffenbaugh and Shivananda had to delete some of the time-dependent terms to obtain bounded solutions. They conjectured that a more accurate scheme would alleviate the problem. To our knowledge, this approach has not been followed upon.

For future work, it seems that the objections to the first approach are deeper than those to the second one. One should be able to formulate a correction at low Mach number. However it is not clear that this can be done without the use of spatial derivatives as in a Poisson equation; these can be handled on a grid, but losing the grid-free character of the method is a heavy price to pay. The best by far would be to find a grid-free strategy for the compressibility correction.

6. INVISCID BOUNDARIES

6.1. Use of Boundary Elements

The traditional way of implementing the inviscid boundary condition (i.e., zero normal velocity at a surface) is by using image vortices. However this is possible only when the shape of the surface is very simple (e.g., straight line or circle) or when one has an analytical conformal mapping from the desired shape to one of the simple shapes. This has led to numerous studies of the flow past circles, ellipses, and Joukovsky airfoils, for instance. Another serious drawback of images in practice is that a vortex close to the wall is also close to its own image. A strong interaction can develop, with the vortex and the image forming a pair and traveling along the wall at a high velocity and in the direction opposite to that of the boundary layer.

In practice the method of boundary elements, in which vortices, sources, or doublets of appropriate strength are placed along the boundary to ensure that the boundary condition is satisfied, is much more flexible. In other contexts it is called the panel method. At the expense of solving a linear system, one can treat arbitrary shapes. The matrix of the linear system is unfortunately full, but in a time-dependent computation it needs to be inverted only once so that the cost at each step is of order M^2 and not M^3 (M being the number of boundary elements).

When the boundary-element method is used as part of a vortex algorithm, as opposed to a potential-flow solver, it is convenient to use vortices for the boundary elements (Lewis, 1981). Furthermore in some cases using vortices is much more natural (for instance the splitter plate for a mixing layer carries a velocity jump and therefore circulation). Let us restrict our attention to 2-D for now. Let the points $\tilde{\mathbf{x}}_j$, $1 \leq j \leq M$, describe the boundary. The bound vortices are placed at these points. One could construct an algorithm to cancel the normal velocity at or near the points $\tilde{\mathbf{x}}_j$ (for instance at $(\tilde{\mathbf{x}}_j + \tilde{\mathbf{x}}_{j+1})/2$). However, there are large local velocities and depending on the exact choice of the test point and other parameters there is a danger of having fluid "leak" through the boundary in the average. It is much preferable to use the stream function: the condition is then $\psi(\tilde{\mathbf{x}}_{j+1}) = \psi(\tilde{\mathbf{x}}_j)$. Thus we are imposing zero mass flux between $\tilde{\mathbf{x}}_j$ and $\tilde{\mathbf{x}}_{j+1}$. This method is more robust, and also more convenient when one has several surfaces (e.g., the walls of a wind-tunnel) and wishes to impose the mass flux between them: the condition becomes $\psi(\tilde{\mathbf{x}}_{j+1}) = \psi(\tilde{\mathbf{x}}_j) - Q$ if $\tilde{\mathbf{x}}_j$ is on one wall, $\tilde{\mathbf{x}}_{j+1}$ is on the other and Q is the mass flux. The stream-function method results in a matrix which is well structured; the largest elements are on the main diagonal and the one just below it, and Gauss elimination without pivoting is sufficient to solve the system.

Typically the stream function results from the linear combination of three components. If there is flow at infinity this corresponds to a stream function $\psi_\infty(\mathbf{x}) = (\mathbf{x} \times \mathbf{U}_\infty).\mathbf{e}_z$ where $\mathbf{U}_\infty$ is the uniform freestream velocity. Note that a slight generalization is possible in 2-D: if the freestream flow has uniform vorticity the vortex method can still be applied to the deviation from the freestream vorticity (i.e., equation (7) still holds, but equation (4) does not in 3-D). Then there is the stream function associated with the free vortices, ψ_f, which is given by (28). The initialization or generation of these vortices strongly depends

on the problem at hand. Finally there is the stream function of the bound vortices, ψ_b, which is given by (28) too. Thus the equations are

$$\psi_b(\tilde{\mathbf{x}}_{j+1}) - \psi_b(\tilde{\mathbf{x}}_j) = \psi_\infty(\tilde{\mathbf{x}}_j) - \psi_\infty(\tilde{\mathbf{x}}_{j+1}) + \psi_f(\tilde{\mathbf{x}}_j) - \psi_f(\tilde{\mathbf{x}}_{j+1}) - Q_j. \qquad (31)$$

The unknowns are the circulations Γ'_j of the M bound vortices. After they have been computed, the velocity of the free vortices is computed and they are advanced for one time step according to (20). The displacement of the free vortices (and possibly the creation of new ones) alters ψ_f, so that (31) has to be solved again for the next step.

The question arises immediately that (31) can be written only for $j < M$; there are only $M-1$ equations, for the M unknowns Γ'_j. This is the well-known paradox: the total circulation is undetermined. The solution is to add an M^{th} equation that prescribes the sum of the circulations. Thus all the elements of the last row of the matrix are 1. Typically, one forces the total circulation in the plane to be zero, so that the M^{th} equation is:

$$\sum_{j=1}^{M} \Gamma'_j = -\sum_{i=1}^{N} \Gamma_i \qquad (32)$$

(recall that N is the number of free vortices). However this condition is not unique; sometimes symmetry or other considerations are applied instead. See the discussion of (38) in §*7.2*.

For the extension to 3-D, one will not have a stream function. One can of course revert to a condition on the normal velocity itself, but imposing the condition in an integral sense as in (31) is preferable. Suppose one has cells on the surface (e.g., triangles); the border of each cell defines a contour. One could use a vector potential and require that its circulation around each contour is zero. This is equivalent to requiring that the flux of the velocity field through each cell is zero. Since mass conservation is built into the discretization, it seems consistent to use for the boundary an algorithm that exactly conserves mass.

An application of the vortex method with inviscid boundaries is given in §*6.3*. Other applications are nozzles or wind tunnels. Spalart (1984) assessed tunnel blockage effects by imposing the inviscid condition on the tunnel walls (on which separation did not occur) and viscous conditions on the body. One can also represent a lifting surface as an inviscid boundary (Katz, 1981), but then the circulation in the lower and upper boundary layers cannot be distinguished, so that one cannot predict viscous effects such as separation; one also needs to impose the Kutta condition.

*6.2. Remark on the Choice of Two Numerical Parameters**

In general, there are no explicit equations linking the different length parameters, so that the user is left with his/her intuition to choose values. However in the simple case of an inviscid boundary one can use the following simple argument to relate the spacing between the points $\tilde{\mathbf{x}}_j$ and $\tilde{\mathbf{x}}_{j+1}$ and the core radius σ. We idealize the boundary as a straight line on the x axis with equally distributed points $\tilde{\mathbf{x}}_j$ at intervals Δ. Let U denote the velocity jump across the sheet. The ideal stream function is $\psi_i = -U|y|/2$; the flow is

uniform at $\pm U/2$ above and below the sheet. With the discretization by vortices, the flow is nearly uniform away from the sheet by forms the usual "cat's eyes" around the vortices. The stream function discretized using vortex blobs with the core function $F \equiv r^2/(r^2+1)$ (see (46)), is given by

$$\psi_d(\mathbf{x}) = -\frac{U\Delta}{4\pi} \sum_{j=-\infty}^{\infty} \log\Big(\frac{|\mathbf{x} - j\Delta\mathbf{e}_x|^2 + \sigma^2}{(j\Delta)^2 + \sigma^2}\Big). \tag{33}$$

The circulation of each vortex is $-U\Delta$, and the denominator inside the logarithm represents an additive constant that was set to ensure that at $\mathbf{x} = \tilde{\mathbf{x}}_j = j\Delta\mathbf{e}_x$, $\psi_d = \psi_i = 0$ (recall that the stream function will be sampled at the points $\tilde{\mathbf{x}}_j$ to write (31)). One can verify that for large $|y|$ the stream function ψ_d given by (33) becomes arbitrarily close to $-U|y|/2 + C$, where C is a constant. The mass flux between the test point $\tilde{\mathbf{x}}_j$ and a point far up will be correct only if $C = 0$. This mass flux is an important quantity when the walls are the walls of a tunnel or nozzle, especially of variable section. It is less important in external flows. A numerical summation of the series (33) showed that $C = 0$ is obtained when σ/Δ is equal to 0.153. The optimum value of σ/Δ naturally depends on the core profile used (the F function). In practice, the value 0.153 can rarely be exactly respected since the spacing of the points is generally uneven, but it is a useful guide.

6.3. Example: a Curved Mixing Layer

Mixing layers, either temporally- or spatially-developing, have been a frequent subject for vortex methods (Ashurst, 1979; Aref and Siggia, 1980; Ashurst and Meiburg, 1985). A short, unpublished study of curved, spatially-developing mixing layers will be described here primarily as an example of how realistic boundary conditions can be applied. The study was suggested by Dr. N. Mansour (NASA Ames Research Center) after some experimental studies showed a strong effect of curvature on the structure of mixing layers (with the faster stream inside, the layer was much more disorganized and three-dimensional).

Although this was not the only way to proceed (see the treatment of the flat mixing layer using two semi-infinite vortex sheets in Leonard, 1980) it was decided to use curved walls as guides for the flow. Let R be the radius of the mixing layer, R_1 the radius of the inner wall and R_2 that of the outer wall. The values chosen satisfied $R_1/R = 0.9$ and $R_2/R = 1.1$, and the "test section" covered one radian (see figure 3). Boundary conditions were enforced on the two walls, on an inflow boundary and on a section of the splitter plate using bound vortices. On the walls and plate, the inviscid no-penetration condition was applied (most mixing-layer simulations do not enforce any condition on the plate; they just place a row of vortices of equal circulation on it). Along the inflow boundary, the velocity normal to the boundary (u_θ) was imposed and equal to the velocity of the irrotational flow (i.e., proportional to $1/r$). This is an example of (31) with $Q_j \neq 0$. It can be interpreted as a porous boundary with imposed blowing. The system was closed by requiring that the circulation of the bound and the free vortices add up to zero, see (32). This value was arbitrary but ensured that the flow outside the walls was relatively quiescent, so that the velocity field was smooth at the inflow and outflow boundaries. Provided that the

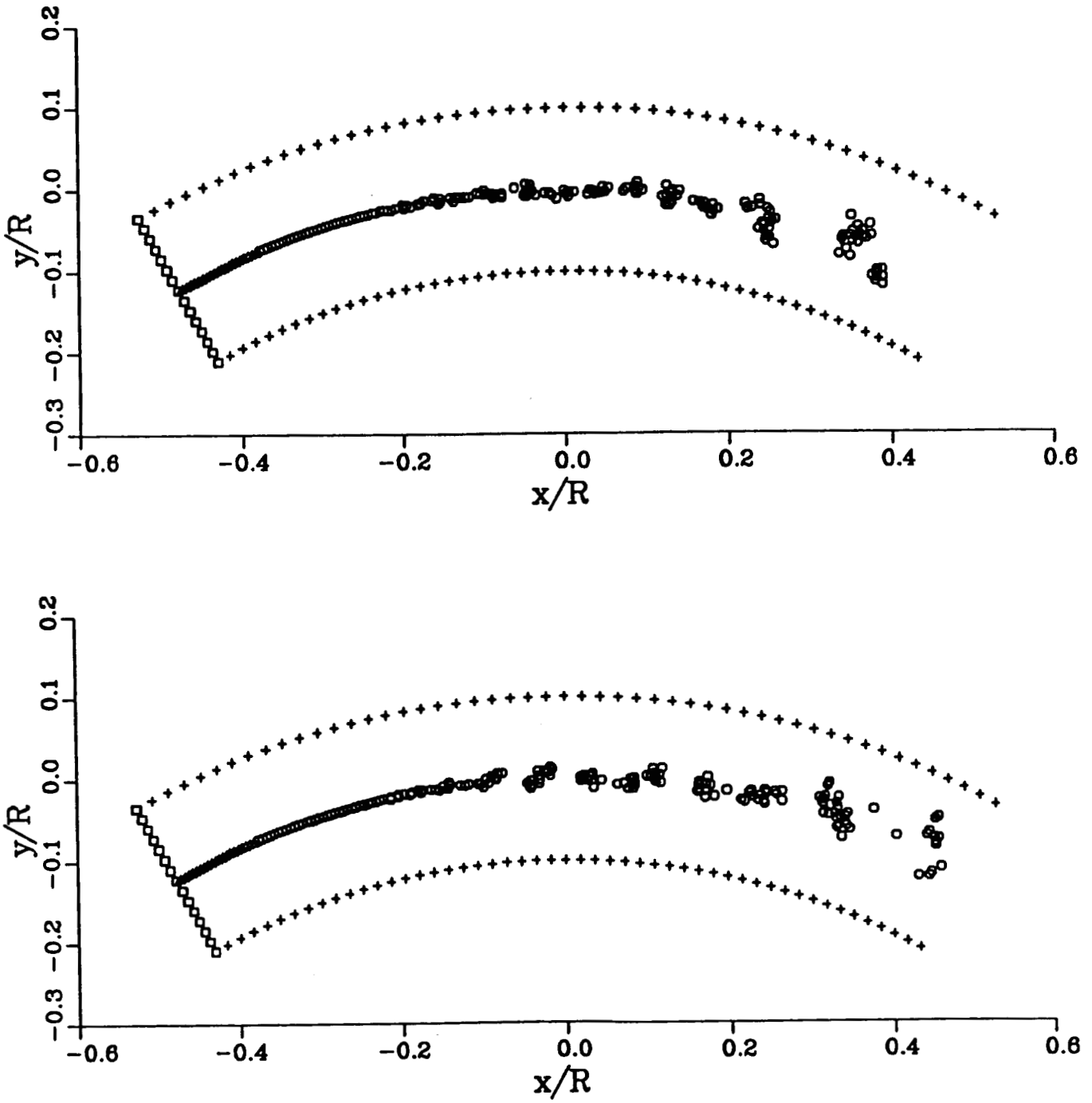

Figure 3. Computation of curved mixing layers. a) Fast fluid outside, $U_2 = 2U_1$; b) fast fluid inside, $U_2 = U_1/2$. ○ free vortices; + vortices bound to walls; △ vortices bound to splitter plate; □ vortices bound to inflow boundary

test section is long enough, the manner in which the linear system is closed (the M^{th} equation) is unimportant, as are the inflow and outflow conditions; here we are invoking Saint-Venant's principle.

No condition was needed at the outflow. The trailing edge of the plate gives an example of a smooth transition from the bound vortices to the free vortices; the two families of vortices have the same spacing, core size, and essentially the same circulation (this assumes the proper relationship between the mean velocity, the time step, and the spacing). At every time step the last bound vortex becomes a free vortex, keeping its circulation. The vortex that is farthest downstream is deleted. Thus the calculation can be run as long as desired.

In parallel with the numerical study, the linear stability of curved vortex sheets was investigated. By generalizing the well-known derivation for flat sheets (Batchelor, 1967, p. 511) it was found that the growth rate a for a wave with wavenumber α is given by:

$$a^2 = \frac{\alpha^2}{4}(U_1 - U_2)^2 + \frac{|\alpha|}{2R}(U_1^2 - U_2^2) \tag{34}$$

where U_1 is the velocity of the inside stream and U_2 is the velocity of the outside stream. Note that this formula reduces to Batchelor's result ($a = \alpha|U_1 - U_2|/2$) as $\alpha R \to \infty$, that is, as the radius of curvature becomes much larger than the wavelength.

Equation (34) shows that the mixing layer is more unstable if the inner stream is faster ($U_1^2 > U_2^2$). However the relative difference in growth rates is smallest for the most unstable waves (largest $|\alpha|$) so this effect is not significant. Figure 3 shows mixing layers with velocity ratios U_2/U_1 of 2 and 1/2 respectively, and confirms that even a significant curvature (compared with the size of the largest eddies) has little effect on 2-D mixing layers. This strongly suggests that the third dimension is necessary to explain the effect observed in experiments.

Another point of interest is that the boundary condition on the splitter plate did not seem to make a noticeable difference in the flow pattern. There was a possibility that the pressure disturbances from downstream would influence the circulation of the new vortex that is created at each step, thus creating a feedback mechanism with the sharp trailing edge as an amplifier. However, in the calculations this effect was very weak, and the flow did not differ noticeably when the boundary condition was enforced using (31) and when the vortices bound to the plate were given uniform circulations.

7. VISCOUS BOUNDARIES

7.1. Application of the Biot-Savart Law Inside a Solid Body

In §6 we showed how the inviscid, no-penetration condition can be conveniently enforced using boundary elements, preferably vortices. We are now interested in satisfying also the no-slip condition. A priori this is more difficult, but we have a very fortunate result that shows that, for external flows, this can still be achieved with a single set of boundary elements (Wu and Sankar, 1980). Thus, calculations with both the no-penetration and no-slip conditions are almost as simple as those with only the former. The key idea is to extend the velocity field and the stream function into the region occupied by the body.

Consider a solid body occupying the bounded region D, with boundary ∂D. It may be multiply-connected, made up of sub-regions D_i. For now we restrict ourselves to a fixed body and 2-D. Suppose we obtained a vorticity field such that the stream function it induces through the Biot-Savart law (8) satisfies the no-penetration condition, $\partial\psi/\partial s = 0$ on ∂D. Recall that (8) represents the Green's function for the whole plane. We may have achieved this using boundary elements; in any case there are only vorticity elements (so that ψ is defined and single-valued), and none of them are inside D. The formula (8) can be applied for $\mathbf{x}$ inside D, and there $\nabla^2\psi = \omega = 0$. Therefore ψ satisfies:

$$\nabla^2\psi = 0 \qquad \text{in } D, \tag{35a}$$

$$\frac{\partial\psi}{\partial s} = 0 \qquad \text{on } \partial D. \tag{35b}$$

This is Laplace's equation with a Dirichlet boundary condition. It is a well-posed problem with a unique solution up to an additive constant in each subregion: $\psi = C_i$ in D_i. Therefore $\mathbf{U}$, as given by (6), is identically zero in D. Also consider $\partial\psi/\partial n$, the normal derivative of ψ as one approaches ∂D *from the inside*. Since ψ is constant in D_i,

$$\frac{\partial\psi}{\partial n} = 0 \qquad \text{on } \partial D, \tag{36}$$

i.e., the tangential velocity just below the boundary is zero. This is a very useful result.

Several remarks. First, one could have first imposed $\partial\psi/\partial n = 0$ and obtained $\partial\psi/\partial s = 0$ as the by-product (Laplace's equation with Neumann condition also has a unique solution up to an additive constant). In other words, if (35a) holds (35b) and (36) are equivalent. In the numerical method we elected to explicitly apply the no-penetration condition $\partial\psi/\partial s = 0$ because it requires less smoothness of ψ (observe that (31) is written directly in terms of ψ, not in terms of derivatives) and also because it seemed more important to conserve mass exactly; the viscous effects, including the no-slip condition, are treated a little more loosely. Second, the solution to (35) is unique only if D is bounded and ∂D is closed, that is, for an external flow. Third, the argument on the normal derivative applies only if one can approach ∂D from the inside, that is, if D has a finite thickness. The argument totally breaks down for an infinitely thin body, e.g., a plate, and in the numerical context

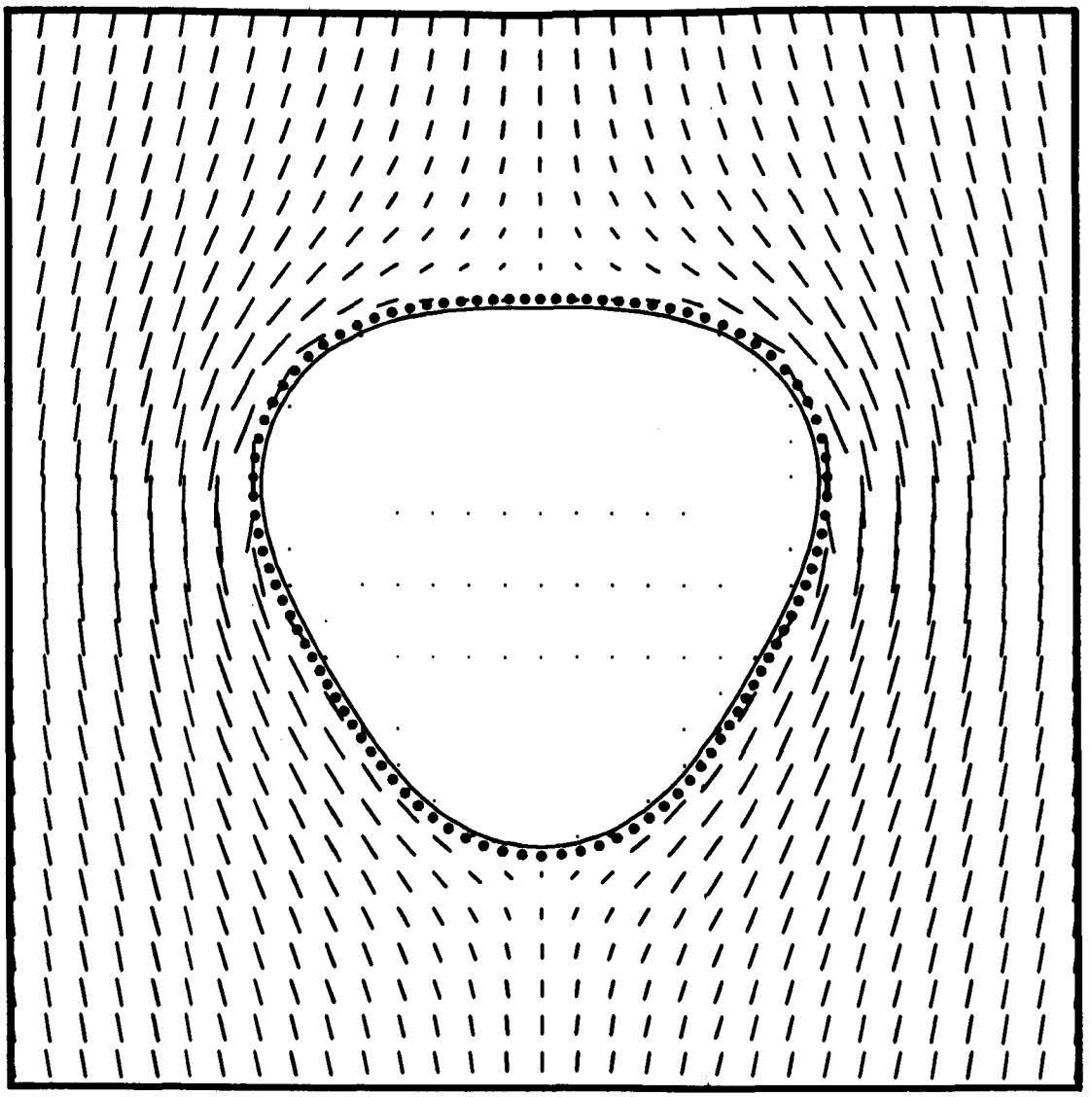

Figure 4a. Flow past a bluff body, just after impulsive start. — boundary; • vortices; ⟶ velocity vectors

one needs to be careful if the thickness of the body is not large enough compared with the spacing of the vortices along the wall.

The behavior of the velocity field is illustrated in figure 4. A simple body shape was considered, just after an impulsive start (i.e., there are no free vortices yet). Thus we have irrotational flow around the body. Boundary vortices were used to enforce the $\partial\psi/\partial s = 0$ condition, discretized as in (31). The velocity vectors computed using (26) are plotted at the nodes of a regular grid, including inside the body. In figure 4a one recognizes the usual potential-flow solution outside the body. Inside the body, the velocity vectors are very small, showing that the formal argument based on Laplace's equation (35) does work

well numerically. This was not entirely obvious, because usually the function δ_σ in (23) does not have bounded support, so that there is a little residual vorticity inside the body, and also because we forced ψ to take the same value (C_i) only at the discrete points $\tilde{\mathbf{x}}_j$ (see (31)). The natural smoothness of solutions to Laplace's equation helps. In figure 4 the boundary elements represent a vortex sheet, and the strength $d\Gamma/ds$ of the sheet gives the velocity jump across the sheet. Therefore $d\Gamma/ds$ gives the tangential velocity *above the elements*. Thus once the boundary vortices are known it is a very simple matter to obtain the limiting velocity of the potential flow at the wall, and the surface pressure through Bernoulli's equation. Thus even for potential flow the method of boundary vortices has a distinct advantage over those based on sources or doublets.

7.2. Creation of Vorticity

The interpretation now differs for inviscid and viscous flow. In viscous flow the vortices along the boundary are not considered as mathematical tools to enforce a boundary condition, but as actual vorticity that is imparted to the fluid by the shear stress at the wall. Solid walls have long been interpreted as sources of vorticity (Lighthill, 1963). New vortices are created at every step and released into the fluid, just like at the trailing edge for the mixing layer (§*6.3*), but now all along the wall (Chorin, 1973). The circulation of the new vortices is computed as is they were bound vortices, but they are immediately considered as free vortices and allowed to move with the fluid. Symbolically, their contribution to ψ is transferred from ψ_b to ψ_f, on the right-hand side of (31), so that $\psi_\infty + \psi_f$ alone satisfies the boundary condition. The vortices then move according to (20), by an amount that is $O(\Delta t)$. This alters $\psi_\infty + \psi_f$ by an amount $O(\Delta t)$, so when (31) is solved again ψ_b and therefore the circulation of the new vortices are $O(\Delta t)$. Thus, a small amount of vorticity is released at each step. The vortices are created not right on the boundary, but a small distance d_0 outside it. There are "wall points" $\tilde{\mathbf{x}}_j$ where (31) (with $Q_j = 0$) is applied, and "creation points", say $\tilde{\mathbf{x}}'_j$ where the new vortices are placed.

The wall points and creation points can be distinguished in figure 4b, which is a detail of figure 4a. Notice the smooth potential flow away from the wall, the velocity vectors becoming very small inside the body, and the transition region in which the direction of the velocity fluctuates. The microscopic description of the wall (on the scale of $|\tilde{\mathbf{x}}_{j+1} - \tilde{\mathbf{x}}_j|$) is a little crude, but on a macroscopic level the method has the following advantage. The row of vortices in figure 4b (and in general with any attached boundary layer) forms a vortex sheet. The tangential velocity above the shear layer is U_e, the velocity of the potential flow, and the velocity below it is zero. Therefore the vortices translate along the wall at a velocity $U_e/2$. This is known to be correct, in the sense that in a boundary layer the average velocity of the vorticity, defined by

$$U_{av} \equiv \int_0^\infty u\ \omega\ dy \Big/ \int_0^\infty \omega\ dy \tag{37}$$

is precisely equal to $U_e/2$ (just use $\omega \approx -u_y$ and an integration by parts). The flux of vorticity along the wall is an important quantity and is correct (as mentioned earlier, it can be very inaccurate when image vortices are used). This is another example of how small-scale errors can cancel each other so that integrated quantities (here, U_{av}) are correct.

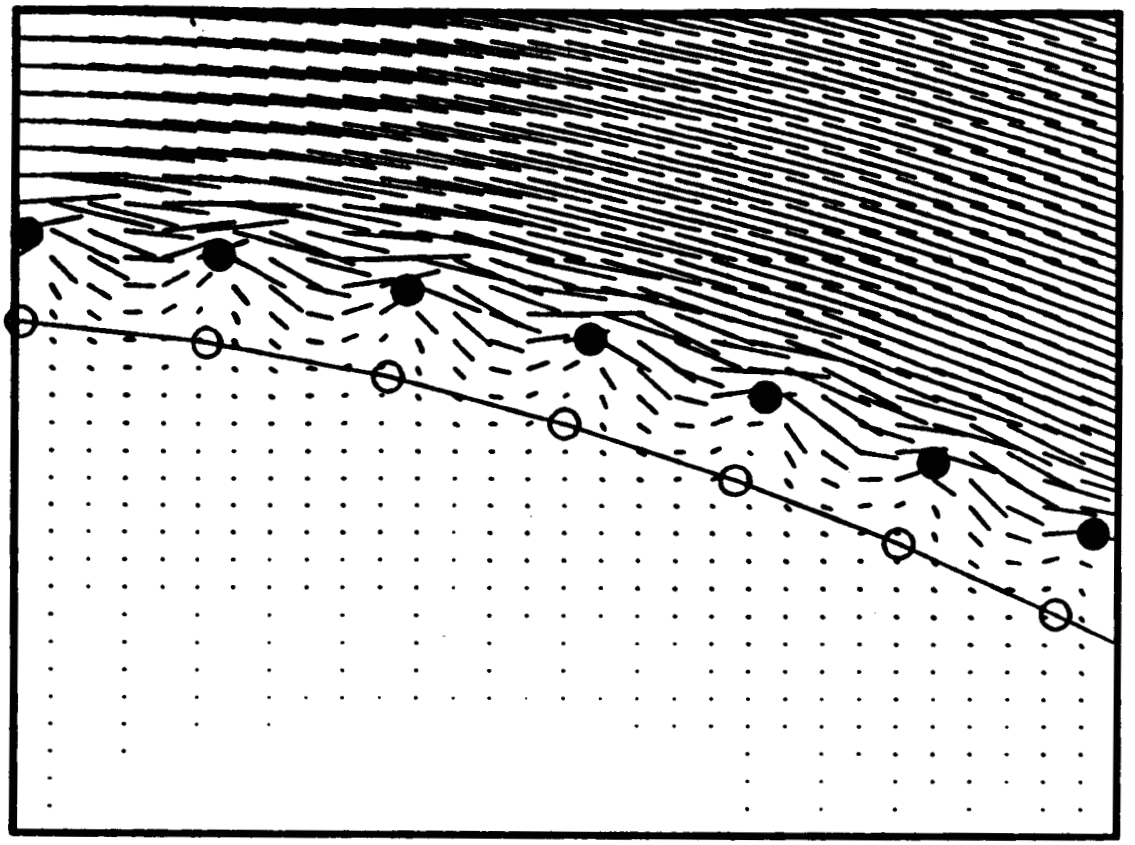

Figure 4b. Flow past a bluff body, just after impulsive start (detail of Fig. 4a).
-o- boundary and wall points $\tilde{\mathbf{x}}_j$; • vortices at creation points $\tilde{\mathbf{x}}'_j$;
$\longrightarrow$ velocity vectors

As in the inviscid flows, we need an extra equation to close the system (31) for each body. This condition is that the circulations of the vortices created along each body at each time step add up to zero (Wu and Sankar, 1980):

$$\sum_{j=1}^{M} \Gamma'_j = 0 \tag{38}$$

Note that this condition is rigorous, unlike (32) which looks the same but was arbitrary (actually, (38) was known and (32) was chosen by analogy). If one considers the whole flow, (38) implies that the total circulation is conserved, a well-known result, see (13). However, (38) is a stronger condition since it applies to each body separately. In summary, for each body described by M wall points there are $M-1$ type-(31) equations and one of type (38). Note that the type-(31) equations are coupled between bodies, so that the whole matrix is full (except for the few type-(38) lines).

In inviscid flow, ω can have a singularity of the order of a 1-D Dirac distribution, and ψ is continuous but with a jump of its normal derivative across ∂D. In viscous flow, ω has

a jump across ∂D but is bounded, and both derivatives of ψ are continuous. Therefore (36) applies on either side of ∂D_i, i.e., the no-slip condition is satisfied. ω is bounded because with viscosity it cannot remain in a sheet; instead it diffuses into the fluid. The mechanism which prevents it from accumulating at the wall is viscous; thus the vortex-creation algorithm is consistent only with a viscous flow solver. In actual calculations numerical effects play a strong role in this process, see §*7.4* and *8.2*.

Several slight generalizations are possible. If the body is translating, this can be taken into account using the Q_j's in (31). If the body is rotating at an angular velocity Ω the situation is a little more involved since there is vorticity $\omega = 2\Omega$ inside D. Again, one adjusts the Q_j's. The stream function induced by the inside vorticity can be computed with the Contour Dynamics formula (Zabusky, Hughes, and Roberts, 1979) and subtracted from the right-hand side of (31). This was done by Spalart and Leonard (1981) for the dynamic-stall study, see figure 7. On the other hand, if the body is deforming or several bodies are in relative motion there is an extra difficulty because the matrix involved in (31) becomes time-dependent, so that it has to be computed and inverted at each step. Finally, in 3-D the same argument as in (35) can be applied to the vector potential. Thus the extension to 3-D is possible, but it has not been made yet; we first need to obtain a robust method for unbounded 3-D flows.

*7.3. Choice of Numerical Parameters**

In the creation algorithm just described, three length scales are involved near the wall. As before (§*6.2*), we have Δ, the spacing between the wall points, and σ, the core radius. Now there is also d_0, the distance from the wall to the creation points. The requirements conflict. d_0 should be large enough compared with σ for the residual vorticity inside the body to be small, but it should also be small enough compared with Δ to maintain a strong coupling between the creation point and the wall point (so that the matrix is well-conditioned). Moreover, σ should be large enough compared with Δ for the cores to overlap in the s direction, so that the velocity field is as smooth as possible (figure 4b). The difficulty arises because the vortices are circular in a region, the boundary layer, where the length scales in the s and n direction are naturally disproportionate. This is partly what motivates separate treatments of the boundary layer (see §**8**).

For viscous flows, a quantitative condition as in §*6.2* has not been obtained; ψ_d cannot be forced to give the right mass flux from $\tilde{\mathbf{x}}_j|$ to ∞ without making the vortex cores impinge on the boundary. In that sense, the actual boundary is blurred, somewhere between the wall points and the creation points. Figure 4b shows a satisfactory set of parameters: $d_0 = \Delta_a/2$, $\sigma = \Delta_a/4$, where Δ_a is an average over the boundary: $\Delta \equiv S/M$ where S is the length of the boundary. The need for a balance between Δ, d_0 and σ implies that the local value of Δ should not have very wide variations. It is helpful to cluster the points (thus reducing Δ) in the regions with high curvature and near sharp corners, but this clustering should be moderate. Typically, Δ should not vary by more than a factor of 2.

7.4. Kutta Condition

The Kutta condition, like conformal mappings and image vortices, is a major tool of classical hydrodynamic theory, and it has been explicitly incorporated in many vortex methods (e.g., Stansby and Dixon, 1982). Actually, a generalization of the classical condition (which just provides the circulation for steady flow on an airfoil with a single sharp trailing edge) was needed since the flows have vorticity and are time dependent, and there may be several sharp edges, like on a square. However the idea is the same: the velocity at any sharp corner must be finite. Note that "Kutta conditions" have been applied to smooth surfaces at separation, which is probably an improper use of the word (in fact, one is just applying the no-slip condition). Note also that a complete viscous method does not need the Kutta condition, because this condition is simply the result of separation of the boundary layers, which an accurate viscous calculation can account for.

It turns out that the method outlined in §*7.2*, with creation of vorticity and the no-slip condition satisfied all along ∂D, does a good job of reproducing this viscous behavior, even when the viscous terms are not included. For instance in figure 1 the flow near the various trailing edges and convex sharp corners is physically correct, although no special treatment or extra condition was applied there. When confronted with a convex sharp corner, the method naturally expels boundary-layer vorticity into the outer flow until a smooth flow without large velocities around the corner is established. The high curvature causes a rapid acceleration and deceleration of the boundary layer, which causes separation. Vorticity is released until the streamline originating at the corner is aligned with the upstream side of the corner.

There are two major reasons for this "pseudo-viscous" behavior. The first is that the vortices are created at a small but nonzero distance d_0 from the wall so that whenever there is a deceleration of the boundary layer they acquire a small velocity component directed away from the wall, which is what initiates separation. The second is that time-integration errors, especially with large velocities and strong streamline curvature, move the vortices away from the wall. The analogies between integration errors and viscous effects are discussed in more detail in §*8.2* and *9.1*. In any case this somewhat fortuitous behavior is consistent, and the flow near sharp edges has always been physically correct. Note that the shedding of vorticity can be only transient as on a starting airfoil without stall, or permanent as in figure 1 or in the case of flow past a square. The separation from smooth surfaces is a much more delicate effect, and is discussed in detail in §8.

7.5. Example: Starting Vortex on an Airfoil

The flow development around an airfoil at incidence started impulsively from rest is considered, and will help clarify the issue of the Kutta condition. This is a classical problem (Prandtl and Tietjens, 1934). The airfoil is NACA 0012; the integral boundary-layer treatment is activated (see §*8.2*) and the Reynolds number is high. Figure 5 shows four snapshots of the flow. At first one sees a sheet of vortices leaving the leading edge and curling up. The starting vortex then grows in size. Since total circulation is conserved, an opposite circulation remains on the airfoil, contained in the boundary layers. A sheet of vortices connects the primary vortex and the trailing edge. This sheet clearly has a nonzero

circulation (velocity jump), since it undergoes a Kelvin-Helmholtz instability. Thus, the circulation on the airfoil is progressively brought up to its final value. In fact, the downwash of the vortex on the airfoil reduces the effective angle of attack, and tends to 0 only like $1/t$. The last snapshot is at much larger time; the wake now has zero circulation (note that it does not roll up any more) and the flow leaves the trailing edge smoothly. The force vector at early times shows a lower lift than in the final state, as well as some drag (induced drag from the starting vortex). At large times the drag is very small.

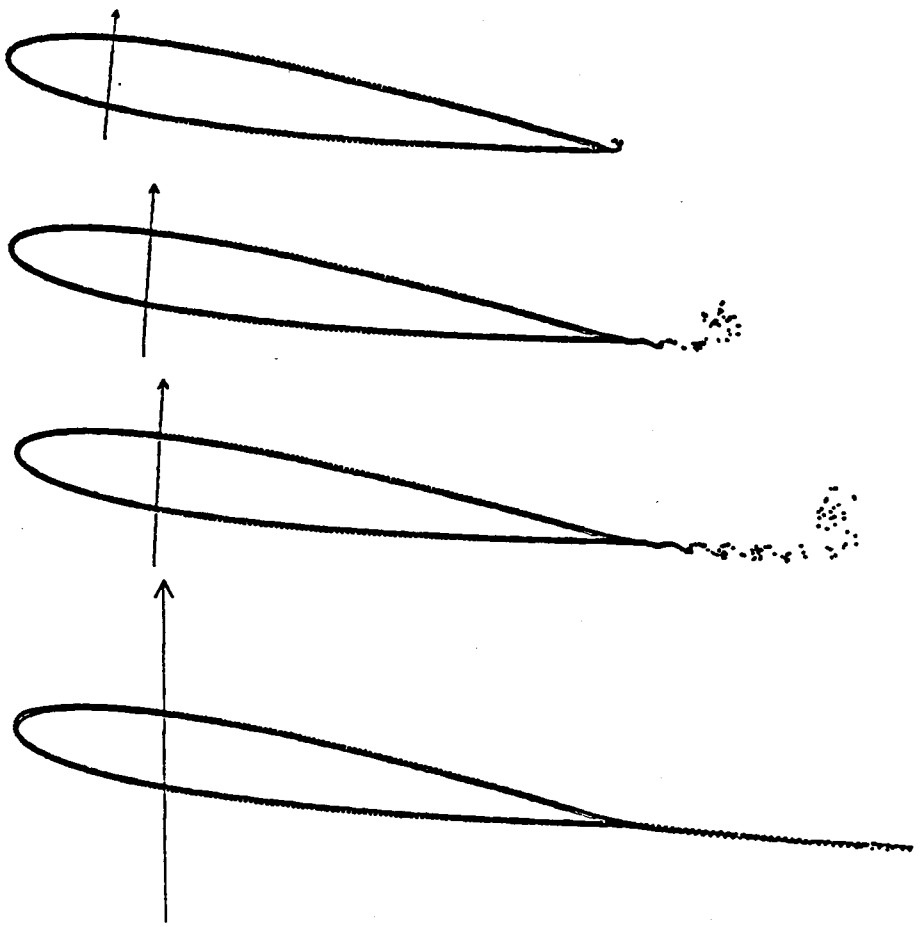

Figure 5. Airfoil starting impulsively without initial circulation. a) $tU_\infty/c = 0.02$; b) $tU_\infty/c = 0.2$; c) $tU_\infty/c = 0.3$; d) $tU_\infty/c \to \infty$. c is the chord and U_∞ the velocity. $\cdots$ vortices; $\uparrow$ force

*7.6. Pressure and Force Extraction**

The pressure was eliminated when the curl of (1b) was taken to derive (4) and is not necessary to advance the vorticity equation, but one often needs it as a diagnostic or for

the treatment of boundary layers. The wall pressure and the forces on the bodies can be obtained directly from the rate of creation of vorticity. Consider a wall with s and n the tangential and normal coordinates. Equation (7) can be written $\omega_t = -\nabla.(\mathbf{U}\omega - \nu\nabla\omega)$, i.e., the flux of vorticity is $\mathbf{U}\omega - \nu\nabla\omega$, which reduces to $-\nu\nabla\omega$ at the wall since $\mathbf{U} = 0$. We take the dot product with the normal vector $\mathbf{n}$ to obtain the flux through the boundary: $-\nu\partial\omega/\partial n$. This is the rate at which the wall is "creating vorticity". Now consider the momentum equation (1b); at the wall it reduces to $\nabla p = \nu\nabla^2\mathbf{U}$ or equivalently $\nabla p = -\nu(\nabla \times \omega)$ (using a vector identity). In 2-D, or in 3-D with a flat surface, one can show that $\mathbf{n} \times (\nabla \times \omega) + \mathbf{n}.(\nabla\omega) = 0$ (in 3-D, curvature seems to introduce another term). In those cases we then get $\mathbf{n} \times \nabla p = \nu\partial\omega/\partial n$, or in 2-D

$$\frac{\partial p}{\partial s} = -\nu\frac{\partial \omega}{\partial n} \equiv \frac{\partial^2 \Gamma}{\partial s \partial t}. \tag{39}$$

The notation $\partial^2\Gamma/\partial s\partial t$ is appropriate since this is a rate of creation of circulation per unit length and unit time. This quantity is known, since we are creating the new vortices at every time step. It is then a simple matter to obtain the wall pressure in 2-D: equation (39) gives us the derivative of the pressure along the wall. We usually apply the trapezoidal rule and write

$$p_{j+1} - p_j = \frac{\Gamma'_j + \Gamma'_{j+1}}{2\Delta t} \tag{40}$$

where the new vortices of circulation Γ'_j and Γ'_{j+1} are created during a step of length Δt.

If we integrate (39) around the wall, since p is single-valued, we get

$$\oint \frac{\partial^2 \Gamma}{\partial s \partial t}\, ds = 0, \tag{41}$$

that is, the total circulation created along each body is 0. This is how (38) was derived by Wu and Sankar (1980). Thus if we apply (38) the wall pressure given by (39) returns to exactly the same value after going around the body, which is not always the case with other methods for computing the pressure. A weakness of (39) is that it gives p only up to an additive constant. In many cases, the front part of the body is in contact with irrotational fluid from upstream; one can then obtain a good estimate of the additive constant by assigning the stagnation pressure to the front stagnation point (this neglects the unsteadiness in Bernoulli's equation). Also, this method does not provide the pressure away from the wall. One could however use this wall pressure as boundary condition for the Poisson equation $\nabla^2 p = -\nabla.(\mathbf{U}.\nabla\mathbf{U})$ (although the additive constants would be troublesome).

The equation $\partial p/\partial s = \partial^2\Gamma/\partial s\partial t$ which led to (40) is much less sensitive to the viscous details of the boundary layer (more specifically, the exact distribution of the vorticity in the normal direction) than $\partial p/\partial s = -\nu\partial\omega/\partial n$ (used by Chorin, 1973). Thus (40) is very well adapted to vortex methods and an accurate wall pressure can be obtained even with a crude representation of the boundary layer itself. For instance if one has a steady attached flow the flux of vorticity along the wall is $U_e^2/2$ as mentioned earlier (§7.2). It is balanced by a flux of vorticity through the wall at a rate $d(U_e^2/2)/ds$; thus we get $dp/ds = -d(U_e^2/2)/ds$,

i.e., the well-known Bernoulli equation. Many procedures have been proposed to obtain the pressure from the time-dependent version of Bernoulli's equation; these methods are very cumbersome in separated flows because of the numerous branch cuts in the velocity potential (one for each vortex).

The global pressure force on a body is given by

$$\mathbf{e}_z \times \oint p(s)\, d\mathbf{l}. \tag{42}$$

After integration by parts and use of (39) this becomes

$$\mathbf{e}_z \times \oint \frac{\partial^2 \Gamma}{\partial s \partial t}\, \mathbf{x}\, ds, \tag{43}$$

which is the negative of (14), applied to the newly created vorticity. This is not a coincidence. Neglect the viscosity for now. What happens is that the motion of the vortices under (26) preserves (14) (the momentum of the fluid), and that the creation of vorticity effects the exchange of momentum between body and fluid. Thus (43) amounts to a global momentum balance (but it can be applied to each body separately). One can check that (43) gives the right "apparent mass" for a body undergoing acceleration. A similar formula holds for the moment on the body, using the invariant (15) (Wu and Sankar, 1980). If the viscosity is not neglected, for instance if a random walk is used, then (14) is not (and should not be) conserved when a vortex collides with the wall, and this is how the friction force comes in. In practice, even without random walk there are such collisions due to noise in the velocity field near the boundary (see §*8.2* and *9.3*) so that the pressure force and the momentum balance do not exactly agree, but this is a small effect, and (39) and (43) have been very satisfactory at high Reynolds numbers.

8. SEPARATE TREATMENT OF THE BOUNDARY LAYERS

8.1. Overview

The boundary layers are the most difficult regions for a vortex method for at least three reasons. First, the standard method uses radially symmetric elements and therefore is not adapted to the disparate scales near the wall (with finite-difference methods, high-aspect-ratio grids are routinely used near the wall). This results in significant noise in the normal component of velocity (recall figure 4b). Second, near the wall the viscous terms become dominant, and the available vortex methods do not treat them very efficiently. Third, the boundary-layer region is usually close to being steady in Eulerian coordinates: $\partial\omega/\partial t$ is small, in contrast with the outer region where it is the Langrangian derivative $D\omega/Dt$ which is small. Thus Eulerian methods have an intrinsic advantage in the boundary layer.

One response to the problem of disparate scales is Teng's (1982) method, which uses elliptic vortices. Teng applied it only to a boundary layer, using identical ellipses and a random walk for the viscosity. He obtained good results, but apparently the method has not been used further. One could certainly extend the idea by using ellipses of different eccentricities; the vortices would be very flat near the wall and circular away from it. The ellipse eccentricity and orientation would be simple functions of the distance to the nearest wall. Note that such a concept is quite different from one in which the ellipse parameters would obey dynamical equations reflecting the straining and the self-induced rotation. The ellipses are introduced for kinematic reasons only; to obtain a more realistic flow field near the wall. A drawback of Teng's method is that the formula for the velocity induced by an elliptic vortex is much more complex than for circular blobs, so that the method can be competitive only if an ellipse can replace at least several blobs. It would pay to find a simpler formula for an "elliptical blob."

Many methods can be found in the literature in which the no-slip condition is not enforced using the boundary elements as described in §7. Most often the no-penetration condition is enforced using images, and there are a few "separation points" at which vortices are created and released into the flow (Lewis, 1981; Stansby and Dixon, 1982). When the body has convex sharp corners, they are obviously going to cause separation, and it is consistent to apply a Kutta condition. The rate of release of vorticity is $U_e^2/2$, with the appropriate sign, where U_e the edge velocity of the upstream boundary layer. This prescribes the circulation of the new vortex, and the Kutta condition provides a condition on its position. Such methods satisfy the intuition and have the major advantage that only a few new vortices are created at every step, compared with hundreds in the method presented in §*7.2*. They are typical of applications on minicomputers. On the other hand, the use of the Kutta condition is still very delicate. Another weakness is that separation, in the sense of a transfer of vorticity from the wall region to the outer region, does not occur only at the obvious points. "Secondary separation" occurs at random on the back face of bluff bodies, and its neglect may be largely responsible for the excess circulation found by some studies and sometimes compensated for by arbitrary means (see §*9.6*). Stansby and Dixon (1982) emphasize the importance of secondary separation. In the long run, and especially for smooth bodies, methods based on a few selected separation points will

probably be superseded by those which allow separation in any region, depending on the boundary-layer dynamics.

The idea of using an inviscid solver for the outer flow and a boundary-layer solver near the wall is old, and has been very successful for attached flows. In such a case one is primarily interested in the viscous friction drag, and possibly in the displacement effect on the outer flow. The trouble starts when the flow separates; the standard boundary-layer equations develop the Goldstein singularity. Any proposal to use the boundary-layer equations for a separated flow should include a discussion of this singularity. It is all too easy to mistake its effects for purely numerical problems, or conversely to suppress them using numerical dissipation.

8.2. Simple Delay of Separation

As mentioned already the vortices induce a fair amount of noise near the wall, which tends to scatter them. As a result, some move away from the wall, and others collide with it. The ones that collide can be pushed back, or they can be absorbed and their circulation be reintroduced a distance d_0 from the wall (see §*9.3*). Statistically, the vorticity tends to drift away from the wall. As soon as there is an adverse pressure gradient, the straining adds to this effect, and separation occurs. This is a mild case of the situation described for sharp edges in §*7.4*. The pure vortex method consistently predicts separation at the onset of an adverse pressure gradient, which is essentially the behavior of a laminar boundary layer. With turbulent boundary layers, separation can take place much farther along the wall and a 2-D method is unable to reproduce this by itself.

This led to the idea of predicting the separation point by a separate method, which can take the Reynolds number and the effects of turbulence into account, and intervening in the dynamics of the vortices to delay their separation up to the correct position. If this intervention is performed in a sensible manner, we can retain the smooth blending between the attached boundary-layer vorticity and the outside vorticity (this is not achieved with the methods that release vortices only at a few points and do not enforce the no-slip condition).

At every time step, the pressure distribution is computed using (40). With it, the two boundary layers starting at the front stagnation point of each body are calculated. So far, only integral methods (Thwaites' and Head's, see Cebeci and Bradshaw, 1977) have been used, in conjunction with Granville's transition criterion, and the time-dependent effects on the boundary layers have been neglected. Thus, there is room for experimentation with more sophisticated boundary-layer solvers. The only information needed from the boundary-layer solution are the separation points (we do not attempt to continue the boundary-layer solution beyond separation). On each body, downstream of these two primary separation points the vortices are free to behave normally, so that secondary separation can take place.

Upstream of the separation points indicated by the boundary-layer solution, we prevent the statistical drift and separation of the vortices simply by re-absorbing the new vortices after only one step. A fresh regular row of vortices carries the boundary-layer vorticity as in figure 4, representing a thin attached boundary layer. Just beyond the indicated

separation point, the vortices are suddenly free and subjected to the straining associated with the adverse pressure gradient, and they leave the vicinity of the wall. This procedure achieves the goal of making the vortices separate approximately in the right place.

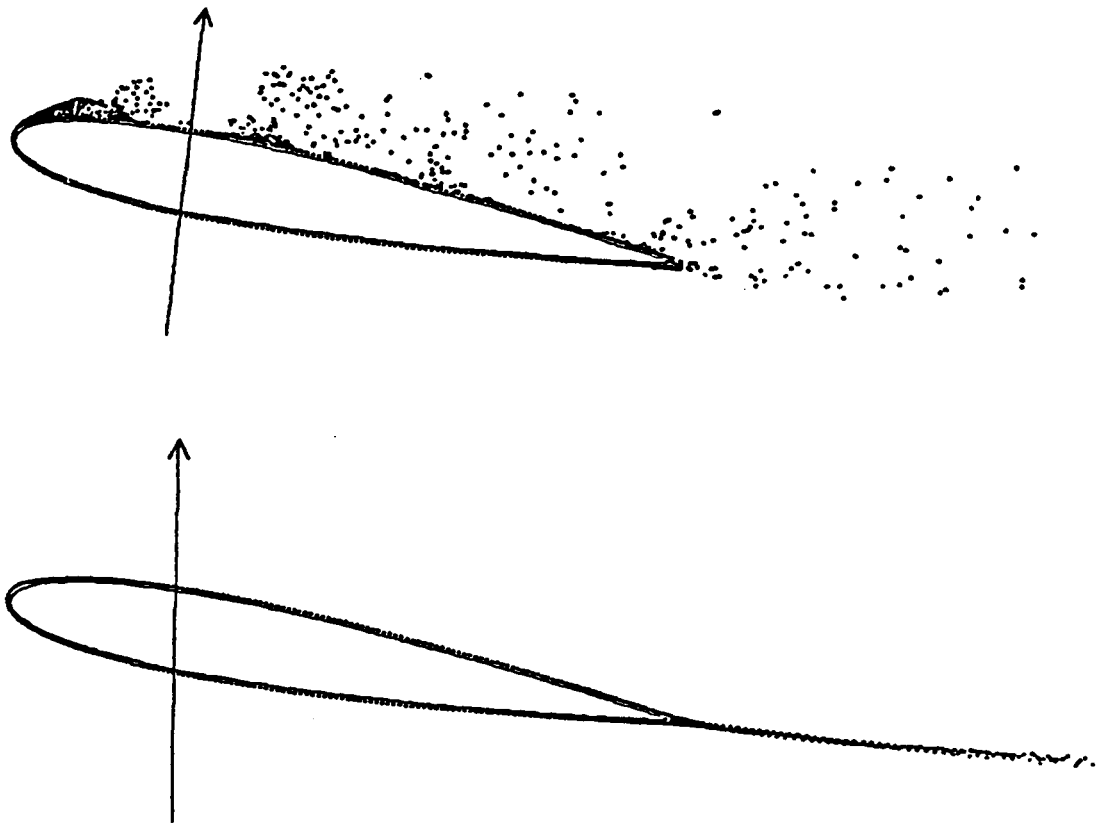

Figure 6. Simulation of the flow over an airfoil. a) without delay of separation; b) with delay. $\cdots$ vortices; $\uparrow$ lift and drag

Figure 6 shows the flow over an airfoil calculated without and with separation delay. In figure 6a, observe how the vortices remain attached on the lower surface, thanks to the favorable pressure gradient, but separate just downstream of the leading edge on the upper surface, in a mild adverse gradient. This is what laminar boundary layers would do. In figure 6b with a very high Reynolds number the integral boundary-layer solvers predicted turbulence, and separation only at the trailing edge. This activated the separation-delay device and we are left with attached boundary layers and a thin, smooth wake. The lift is higher, and there is almost no drag. Separation delay was also applied in figure 1; it made a difference on the upper surface of the slat, and on element 4. It was fully responsible for the Reynolds-number dependence that was described (§*1.1*).

This device has been used extensively, and is very helpful in many cases (figures 1, 5,

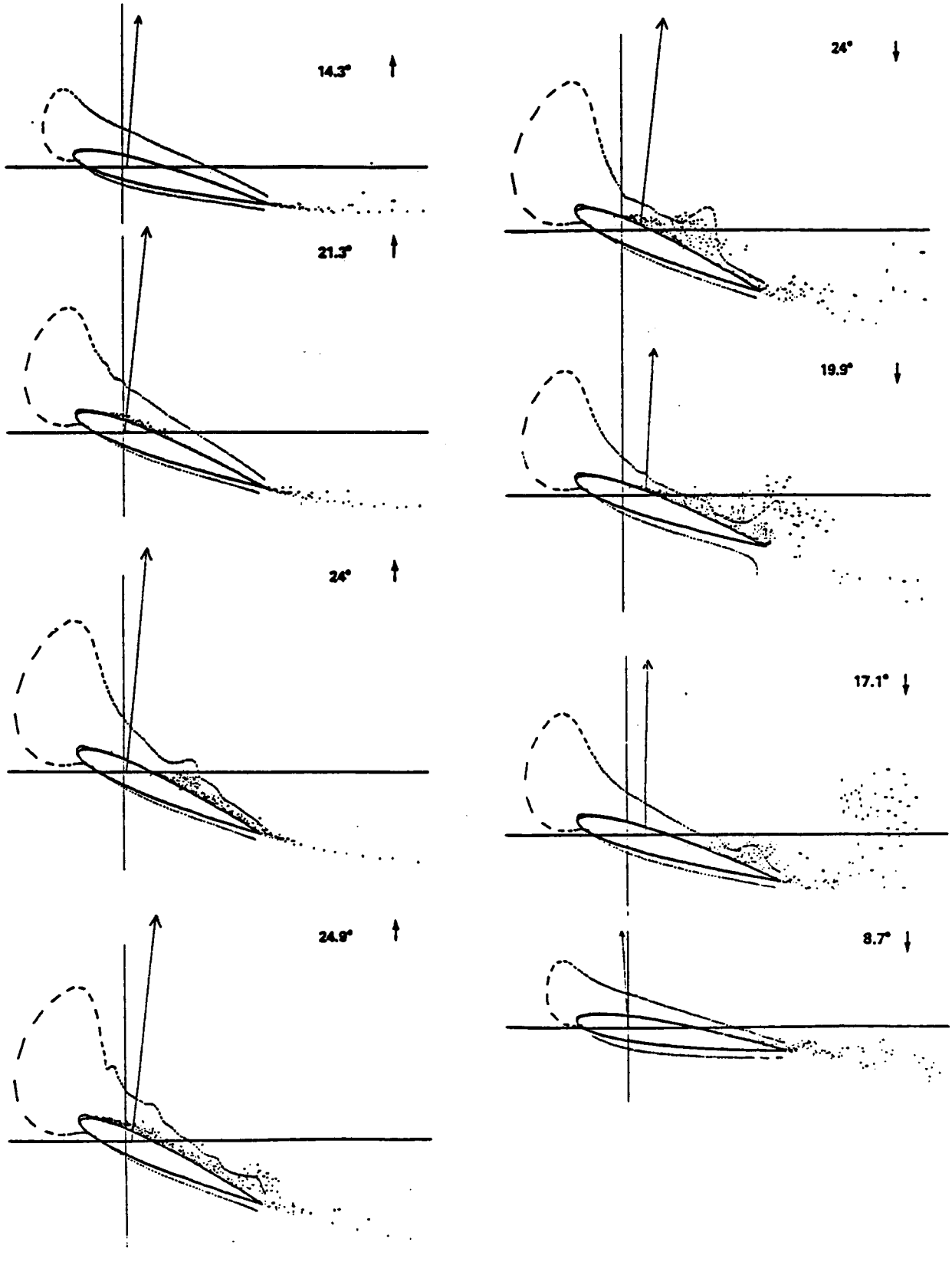

Figure 7. Dynamic stall of an airfoil ··· vortices; ↑ forces. - - - pressure distribution

6b, 7, 13 and 14), but it also has weaknesses; it cannot account for reattachment. The weakest part of the solution is the transition prediction (but this is true of any method). To obtain a flow pattern that agreed with experiment in figure 7, the transition criterion had to be adjusted; the increase in R_θ from the instability point to the transition point was taken as half of Granville's correlation. Another minor problem occurs when one cannot find the front stagnation point because the flow is too disturbed in front of the body. This occurs in the rotating-stall calculation, see figure 14. In that case, one just bypasses the boundary-layer solution for this body at this step. Finally, the integral methods have a tendency to predict separation a few wall points downstream of sharp corners, and one needs to override this prediction and set the vortices free a few points upstream of the corner. Because of these issues, when starting with a new shape it is good practice to first simulate the flow without separation delay, then activate the device if there is a need for it, and carefully check the behavior of the boundary layers.

Figure 7 shows a case in which separation delay made a significant difference. An NACA 0012 airfoil is oscillating from 5° to 25° at a reduced frequency of 0.25 (Spalart and Leonard, 1981). The overall flow strongly depends upon separation on the upper surface just behind the leading edge, and this separation is controlled by transition in the boundary layer. The Reynolds number was 2.5 10^6. The forces and moments on the airfoil were in very good the agreement with experiments (Spalart, Leonard, and Baganoff, 1983).

*8.3. Chorin's Tile Method**

In 1978 Chorin introduced a vortex-like method for the boundary layer. As before, the elements carry circulation, move with the fluid, and undergo a random walk for viscous diffusion. However they are now "sheets" or "tiles" and the velocity is computed in a much simpler manner thanks to the boundary-layer approximations (the tiles interact only with their neighbors). This method is much cheaper computationally than the usual method or Teng's method (1982), and is designed for use in a hybrid algorithm, with conventional vortices away from the wall. Circulation is exchanged by the two subdomains, primarily in the direction sheet $\rightarrow$ blob. Chorin discusses the Goldstein singularity and the need for a viscous-inviscid coupling strategy to remove it, but the subsequent users of the tile method completely overlooked this issue.

Cheer (1983) applied the complete hybrid method to the flow past a circle and Joukovsky airfoils, with Reynolds numbers of about 1000. She obtained flows with "laminar" behavior, i.e., separation as soon as the boundary layer enters the adverse pressure gradient, and satisfactory drag and lift values. Ghoniem and Gagnon (1987) applied it to an internal flow at rather low Reynolds numbers, which seems a little superfluous since there were no thin boundary layers (the inflow was a parabolic profile); quite probably a pure vortex-blob method would do just as well. In summary, the tile method succeeded in introducing the boundary-layer character for the near-wall flow; it is fast and solves the first problem described at the beginning of §8 (the scale disparity), but not really the other two. The convergence of the random-walk method is rather slow here as it is with blobs. Also, the Goldstein singularity is a major problem and Chorin himself (1978) did not assert that it was fully solved.

*8.4. Coupling with a Finite-Difference Solver**

As mentioned above, Eulerian methods have significant advantages for boundary layers, especially if they are steady or quasi-steady, which makes the time integration undemanding. Furthermore, the location of the steep gradients is known and it is easy to cluster the grid points near the wall. This motivated an effort to couple an inviscid vortex solver, for the outer region, and a finite-difference solver, for the wall region (Spalart, Leonard, and Baganoff, 1983).

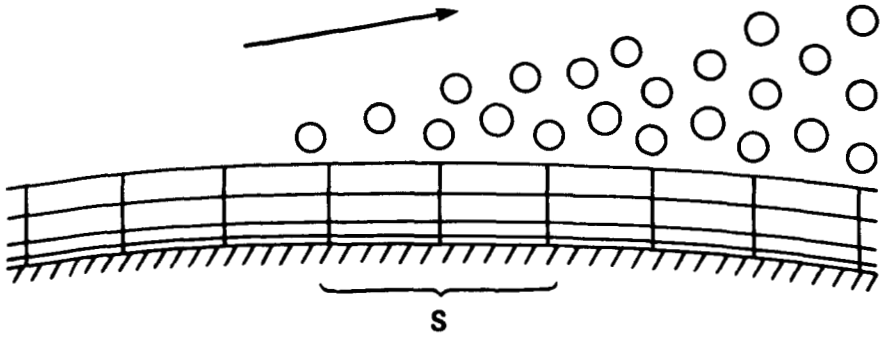

Figure 8. Sketch of the hybrid finite-difference/vortex algorithm. o vortices; — grid lines; ⟶ velocity

The inner region is a thin strip along the wall, see figure 8. The boundary-layer vorticity equations are solved using a standard, implicit, centered finite-difference scheme (T. Pulliam, personal communication, 1981). Simple transition and turbulence models are used. The challenge is in the coupling with the outer region. The two regions exchange circulation as in the tile method, according to the direction of the velocity at the interface. The coupling of the velocity fields is more delicate. A viscous-inviscid coupling was implemented based on the displacement thickness (the centroid of the inner-region vorticity). The procedure is intuitively correct and very similar to the ones used in attached flows, but there is no proof that it actually removes the Goldstein singularity, especially when large amounts of vorticity cross the boundary. Some numerical difficulties (oscillations) in the separation region suggest that it does not (see Spalart *et al.*, 1983, for details). Partly for this reason, this method has not been as robust, and has received much less use than the simpler "delay" method (§*8.2*).

The method however gave encouraging results for the flow past a circle. The "drag crisis" in this flow at Reynolds numbers near 3×10^5 is one of the major challenges in the field of viscous flows. The flow was calculated for Reynolds numbers between 10^4 (the lower limit for thin boundary layers to form) to 3×10^7 (beyond which there were

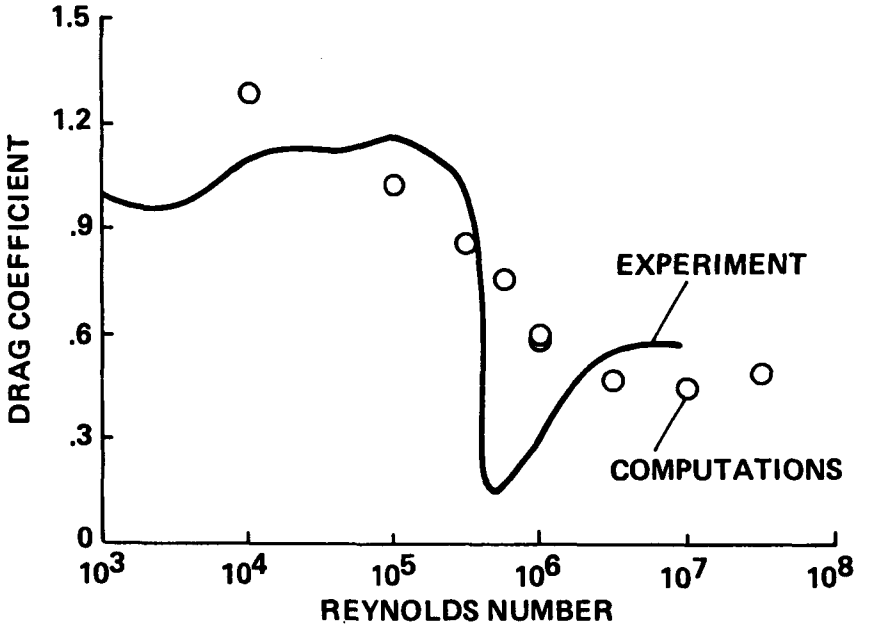

Figure 9. Drag coefficient of a circular cylinder. — average of experiments; o calculation

no experiments). Figure 9 shows that a decrease in drag coefficient was observed, but that the crisis itself (including the sudden drop to very low drag values and the steady lifting states observed in experiments) was not. The drag decreased at higher Reynolds numbers because the boundary layers transitioned; the turbulence model then kept the vorticity attached longer, so that it crossed the boundary into the outer region farther downstream. This is illustrated in figure 10; the mean streamlines, shown at $Re = 10^5$ and 10^6, reflect the position of the separation region. By symmetry, only half of the flow needs to be shown. The Reynolds-number effect was qualitatively correct, and the quantitative agreement with experiments, over a wide range of Reynolds numbers, was fair.

For the future, the use of an Eulerian solver for the inner region should be the most efficient procedure. On the other hand, it is not the most elegant since it is a hybrid, and the coupling and singularity issues definitely need to be re-examined. One could of course solve the full Navier-Stokes equations in the inner region; the obstacle there is that one would need to solve a Poisson equation to obtain the velocity field, instead of just integrating the equations $u_y = -\omega$ and $v_y = -u_x$ up from the wall. The velocity boundary condition on the interface would be a serious problem.

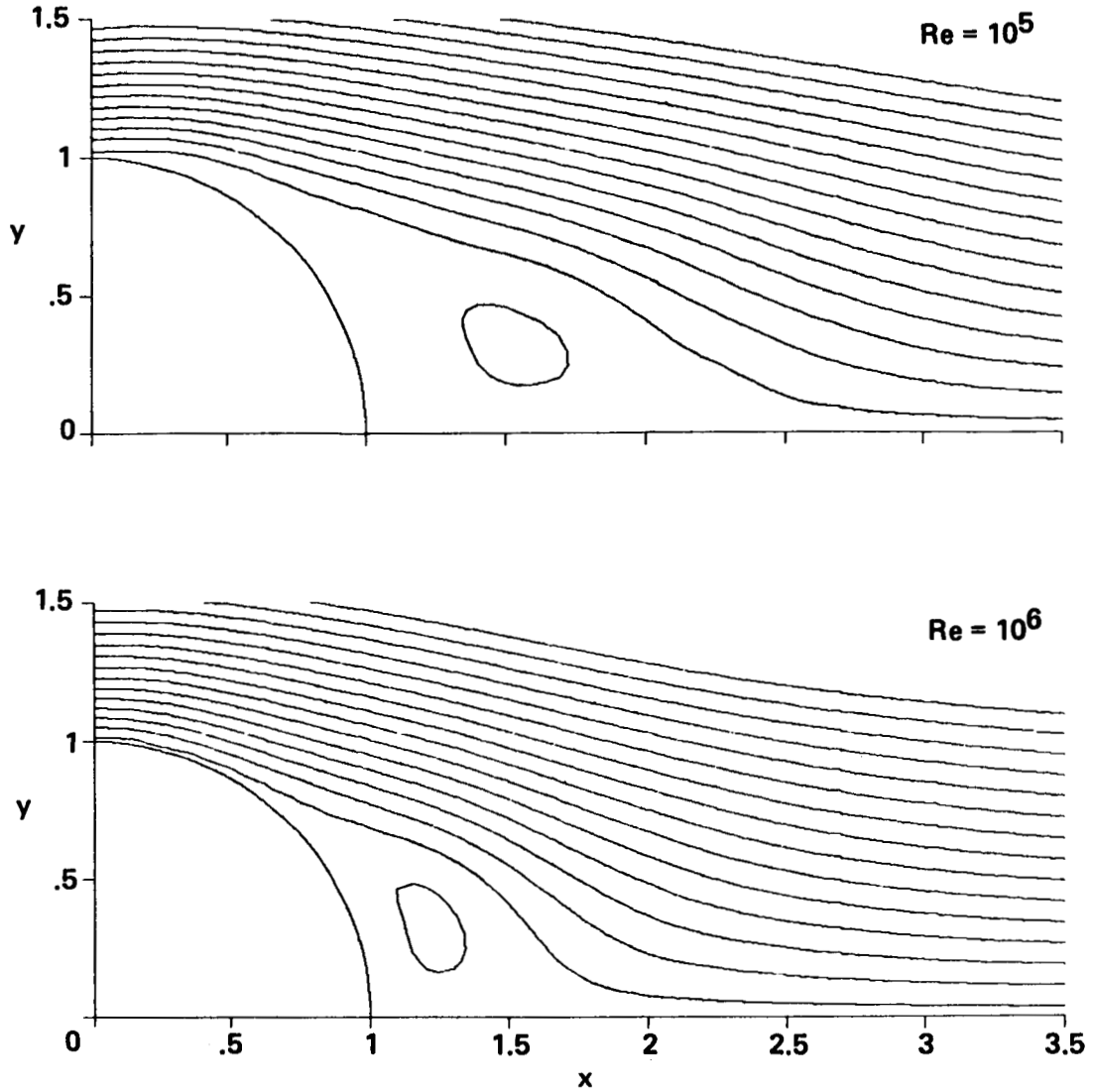

Figure 10. Mean streamlines past a circular cylinder. a) $Re = 10^5$; b) $Re = 10^6$

9. PRACTICAL ASPECTS

9.1. Time-Integration Schemes

A wide variety of time-integration schemes are used in computational fluid dynamics, and the choice is often a matter of taste in addition to the technical concerns. Still, one can narrow down the choice considerably in the case of vortex methods. The first point is that all the schemes used have been explicit schemes. To use an implicit scheme one would need to invert (26) or at least a linearized form of it, and (26) is too complex for this to be done efficiently. Moreover the usual stability advantage of implicit methods is much less crucial with vortex methods than with grid-based methods (see below). The second point is that the most costly part of the algorithm, by far, is the evaluation of the time derivative using (26). Also, the calculations use a relatively small amount of memory, so that storing old values of the time derivative is not a problem. This suggests that multi-step schemes are preferable to predictor-corrector schemes.

Based on these remarks the author has used the Adams-Bashforth second-order scheme,

$$\mathbf{x}_j(t+\Delta t) \approx \mathbf{x}_j(t) + \Delta t\left(\frac{3}{2}\mathbf{U}(\mathbf{x}_j,t) - \frac{1}{2}\mathbf{U}(\mathbf{x}_j,t-\Delta t)\right) \tag{44}$$

for the integration of (20), which represents a good compromise between accuracy, simplicity and cost. As usual, the first step for each new vortex is done using the Euler scheme. A majority of the studies in the literature used either the Euler first order scheme or Runge-Kutta schemes of second or fourth order (the Runge-Kutta second-order scheme is also known as "modified Euler" or "Huen's scheme"). The use of the low-order Euler scheme, when the Adams-Bashforth scheme is hardly more costly, was motivated either by a question of consistency with the random-walk algorithm (in Chorin's method) or by a faulty concept of numerical dissipation, as discussed below.

The integration of (20) is most difficult when large accelerations are experienced by a vortex, typically when it is close to another vortex. Therefore a good model problem is the motion of just two vortices (Spalart and Leonard, 1981). The problem can be expressed in complex notation and simplified to

$$\frac{dz}{dt} = \frac{i\Omega}{z^*}, \tag{45a}$$

$$z(0) = 1 \tag{45b}$$

where z is the separation vector between the two vortices, z^* is its conjugate and Ω is a frequency. The exact solution is $z = \exp(i\Omega t)$: the vortices orbit around each other with angular velocity Ω. Their distance is constant. It is a good exercise to program (45) and observe the behavior with different numerical schemes.

One finds that with any scheme, if the time step Δt is large compared with $1/\Omega$ the solution is inaccurate. However due to its nonlinearity (45a) reacts very differently from the linear equations that are usually studied, e.g., the equation $dz/dt = i\Omega z$ which has the same exact solution. Usually, as an explicit scheme becomes inaccurate (because Δt

is too large) it also becomes unstable and the solution grows to infinity (it "blows up"). With (45a) the distance between the vortices grows until $|z|^2/\Omega$ is of the order of Δt, then settles down. The vortices now orbit at a lower angular velocity, $\Omega/|z|^2$. With some schemes $|z|$ will shrink again and in some cases one gets an oscillation, especially with multistep schemes as the primary and spurious roots alternatively dominate (Spalart and Leonard, 1981). With the Adams-Bashforth scheme, such unphysical behavior has not been observed.

The lesson to be learned here, which holds in practice with many vortices and has been recognized by many authors (Milinazzo and Saffman, 1977, etc.), is that in almost all situations time-integration errors tend to scatter the vortices. The scattering occurs whenever the local rotation rate Ω is large compared with $1/\Delta t$ and corrects itself, since the scattering precisely reduces Ω. The corollary is that a sustained instability, with the solution "blowing up" to infinity, never occurs. In that sense, the method is "robust". However, a solution can remain bounded and be very inaccurate. Also, a scattering of vorticity reduces the velocity fluctuations and the kinetic energy. In that sense, it represents a numerical dissipation. Lagrangian methods, unlike fixed-grid Eulerian methods, allow a perfect convection of flow structures by a *uniform* velocity field; however when gradients are present inaccuracies show up as with any other method.

The scattering of vortices has implications for the invariants (11, 12, 15, 16). The total vorticity (9, 13) and the impulse (10, 14) are linear quantities in terms of the vortex positions $\mathbf{x}_j$. Therefore with the common time-integration schemes which are all linear, if (9, 10, 13, 14) are conserved by the spatial discretization they are still conserved even allowing for time-integration errors in (20). This is not so for the nonlinear invariants (11, 12, 15, 16); they are only "semi-conserved" and have often been used as measures of the integration errors. For example Nakamura, Leonard, and Spalart (1982) defined a global measure of the numerical dissipation, an "effective viscosity," based the time evolution of (15), primarily to verify that it was purely caused by time-integration errors (indeed, it was). Some researchers pushed this reasoning one step too far, concluding that time-integration errors were desirable, since they introduce the viscosity that is so difficult to introduce by other means! They then use the most inaccurate and dissipative (when applied to (45)) scheme, the first-order Euler scheme. Nakamura *et al.* never implied that the effective viscosity had any meaning locally. Moreover, if errors are what one is after, it is cheaper to just increase the time step, rather than switching to a lower-order scheme.

One final remark about steady flows. If the velocity field is naturally time independent, grid-based methods can usually find the solution faster by direct solution or by relaxation techniques than by a straightforward integration in time. Vortex methods do not have this option and treat any flow as time dependent; the vortices move even in a steady flow. Fortunately, most separated flows are strongly unsteady, so this difference is not of much importance in practice.

9.2. Core Functions

In a separated-flow calculation one will need to compute F and $\tilde{F}$ many times, so that it is desirable for both to have simple formulas. Consequently it is convenient to choose $\tilde{F}$

first. As mentioned earlier the Gaussian core (21) (but with a fixed radius σ substituted for $\sqrt{\nu t}$) is attractive but is expensive to compute, and yields only second-order accuracy. A very simple core profile was used in all the cases shown in these notes:

$$F(r) \equiv \frac{r^2}{r^2+1}. \tag{46}$$

It is second-order accurate too. Its only weakness is that the vorticity decays rather slowly at large distances, like r^{-4}, so that the residual vorticity mentioned in §*7.3.* is not negligible. A vorticity distribution with bounded support or at least faster than r^{-4} decay would be preferable as far as the interaction with walls is concerned. Hald (1979) and Beale and Majda (1982, 1985) give formulas for higher-order cores. Recall that Perlman (1985) found that these performed better only if the vortices remained well-ordered, so that in complex separated flows their advantage is probably marginal.

9.3. Control of the Vortex Count

In most applications, many new vortices are created at every time step and added to the list. For instance in the calculation of figure 1, there are about 1300 vortices in total, and 249 new ones are created along the wall at each step. Clearly, useful calculations are possible only if vortices are deleted at about the same rate they are created.

First take the simple case of the mixing layer of figure 2. At each step, one new vortex is created at the trailing edge, and one "old" vortex is deleted near the outflow boundary. The easiest procedure is to delete the oldest vortex; a slightly better one is to delete the vortex that is farthest downstream. This makes little difference, because the last 10 or 20% of the domain are not included in the "measurements" (e.g., velocities, Reynolds stresses) anyway since that region is disturbed by the lack of vortices beyond the outflow boundary. Either method allows one to generate a satisfactory statistically steady state of the flow, and to maintain it as long as desired.

In the less simple cases with solid bodies, two operations allow one to control the number of vortices. The first one is the absorption of vortices by the wall. When a vortex collides with the wall, one has several options. One can reflect it as in an elastic collision, or just push it back to the wall. A third option which is consistent with the treatment of viscous boundaries described in §*7.2* is simply to delete the vortex. If this is done before the evaluation of ψ_f for (31), the right-hand side of (31) will reflect the loss of circulation near the wall, and the new vortices will make up for it (also adjust the last line of the right-hand side, (32)). This absorption procedure has the advantage of helping to contain the number of vortices, and of slightly reducing the noise near the wall.

The absorption of vortices is helpful, but is not enough since it is not under the user's control; a majority of vortices still leave the vicinity of the wall and move into the wake. Thus one needs a more active and adjustable means of limiting N. This can be done by merging vortices. The method used is adapted from Rogallo's (personal communication, NASA Ames Research Center, 1979). Deffenbaugh and Marshall (1976) also used a simple merging device. At every step, pairs of vortices are merged into single vortices. The goal is to achieve this with the least amount of modification of the velocity field.

Since a large local modification is unavoidable, it makes sense to require that the velocity in the far field be altered as little as possible. Suppose the vortices j and k are merged, and the new vortex is given the circulation Γ' and the position z'. Using complex notation and omitting some constant factors, the change in the velocity at z is:

$$\frac{\Gamma'}{z-z'} - \frac{\Gamma_j}{z-z_j} - \frac{\Gamma_k}{z-z_k}. \tag{47}$$

The Taylor expansion for large $|z|$ is

$$\frac{\Gamma' - \Gamma_j - \Gamma_k}{z} - \frac{\Gamma' z' - \Gamma_j z_j - \Gamma_k z_k}{z^2} + \frac{\Gamma' z'^2 - \Gamma_j z_j^2 - \Gamma_k z_k^2}{z^3} + O(|z|^{-4}). \tag{48}$$

The two leading terms are removed by taking $\Gamma' = \Gamma_j + \Gamma_k$ and $z' = (\Gamma_j z_j + \Gamma_k z_k)/\Gamma'$: the new vortex inherits the sum of the circulations of the old ones, and is placed at their centroid. This could be expected; the circulation (13) and the vortex centroid (14) are conserved. On the other hand, (15) and (16) cannot be conserved (recall that they were already not conserved because of time-integration errors).

The next term in (48) cannot be removed and we take it as the merging criterion, i.e., we merge a pair only if this term is below some tolerance. After insertion of Γ' and z' and taking of the modulus it becomes:

$$\frac{|\Gamma_j \Gamma_k|}{|\Gamma_j + \Gamma_k|} \quad \frac{|z_j - z_k|^2}{|z|^3}. \tag{49}$$

Consider the two factors in this estimate. The first one encourages merging of weak vortices (small Γ_j and/or Γ_k), which is sensible since weak vortices cost as much as strong ones, but carry less information. It also discourages merging of vortices with nearly opposite circulations (small $|\Gamma_j + \Gamma_k|$) which also makes sense since in such a merging z' ends up far away from z_j and z_k which is not natural.

The second factor encourages merging of close vortices (small $|z_j - z_k|$) as one would expect. We still need to prescribe $|z|$ in the denominator. The most sensitive place in the flow is the wall region; therefore we insert the distances d_j and d_k from the vortices to the closest wall. The formula that was finally adopted is

$$\frac{|\Gamma_j \Gamma_k|}{|\Gamma_j + \Gamma_k|} \quad \frac{|z_j - z_k|^2}{(D_0 + d_j)^{3/2}(D_0 + d_k)^{3/2}} < V_0. \tag{50}$$

Notice how the formula was symmetrized with respect to d_j and d_k. The length parameter D_0 allow one to shift resolution closer to the walls (small D_0) or into the wake (larger D_0), but the calculations show little sensitivity to D_0 over a wide range (Spalart, Leonard, and Baganoff, 1983). A typical value is 10% of the chord.

Finally, the quantity V_0 in (50) has the dimensions of a velocity and is the tolerance. Typical values are small: less than 10^{-4} times the freestream velocity. In practice it is most convenient to let the program adjust V_0 during the run. One chooses a target number of

vortices, and employs a feedback mechanism that raises V_0 if there are too many vortices, and vice-versa. The merging procedure described here has been very convenient in practice, is intuitively correct and has a rational basis in the Taylor expansions. On the other hand, merging is a very noisy operation locally, and its effect on the convergence is unknown. Therefore, it is not appropriate for all applications.

9.4. Efficient Programming; Operation Counts

Vortex codes are relatively easy to optimize, because almost all the operations are spent computing the N^2 interactions in (26). Thus one really needs to optimize only about ten lines of code. There are a number of nearly-obvious tips. The division by 2π and the $\times$ product should be done outside the $O(N^2)$ loop. The formulas for the two interactions, $k \to j$ and $j \to k$, have a lot in common, namely the computation of

$$\frac{(\mathbf{x}_j - \mathbf{x}_k)}{|\mathbf{x}_j - \mathbf{x}_k|^2} F\left(\frac{|\mathbf{x}_j - \mathbf{x}_k|}{\sigma}\right) \tag{51}$$

After this, the circulations Γ_k and Γ_j are presumably different and the overlap ends. One should have an outer loop ($k = 2, N$) and an inner loop ($j = 1, k-1$) and compute (51) only once. There is no need to store it (which would occupy N^2 words of memory); use it right away to increment $\mathbf{U}_k$ and $\mathbf{U}_j$ (or store all the $j \to k$ terms and sum them up outside the j loop but inside the k loop). In 2-D there is no need to compute any square root, and one can avoid exponentials. The operation count is $8N^2$ with the simplest core, (46), and would be hardly higher for more complex but algebraic cores. In 3-D, the symmetry between $k \to j$ and $j \to k$ is useful too. One should also precompute quantities like the tangent vector outside the $O(N^2)$ loop.

In practice, periodic calculations could be much more expensive than unbounded ones, because the stream function and its derivatives involve the computation of several complex exponentials N^2 times (see §*10.1*), and exponentials cost many floating-point operations. However, this drawback can be completely eliminated with a little extra programming. One needs the values of $\exp(i\pi(z_k - z_j)/p)$ for all values of k and j. What one does before entering the $O(N^2)$ loop of the program is to precompute and store $\exp(i\pi z_k/p)$ and $\exp(-i\pi z_k/p)$ for every k. Then the operation that is done N^2 times is $\exp(i\pi z_k/p) \times \exp(-i\pi z_j/p)$: the exponentials have been eliminated. This can easily speed up the execution by a factor of 4 or more, depending on the computer. In fact, the $O(N^2)$ component of the operation count is only $18N^2$ so a well-programmed periodic method is only about twice as expensive as the unbounded-flow method. Thus there is no reason to approximate (52) by taking the first few terms in the series, as has sometimes been done in the past. The same trick applies to the computation of the stream function ψ_f at the wall points, for (31).

Another tip concerns the use of complex variables, in 2-D. They are convenient, but degrade the efficiency of some computers to some extent (the machines that slow down when the loops have skips of 2). Some machines even refuse to vectorize any loops involving complex variables. This should be checked carefully before writing a code.

9.5. Flow Charts

Here we give flow charts of two programs, named KPD1 and KPD2. Both are available from COSMIC (a part of NASA) in the U. S., as are their periodic counterparts for cascades. A listing of KPD1 also is included in the author's thesis (Spalart, Leonard, and Baganoff, 1983) (there is an error on line 15, p. 107; replace NW by NWALL(L)). KPD1 is the basic bluff-body code with no boundary layer treatment; KPD2 has the integral-method treatment of the boundary layers (the "separation delay" of §*8.2*). The flow charts provide an overview of the material covered until now, and specify the order in which the various operations are performed.

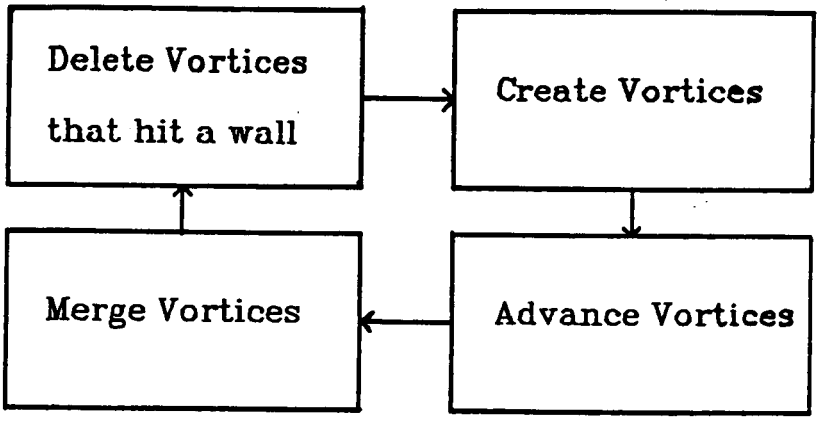

Figure 11. Flow chart of the KPD1 code

9.6. Assessment of the Accuracy

This can be delicate in practice. Some numerical methods (in particular with explicit time-integration schemes) give the user a strong warning when the time step is too long: they "blow up". Other methods (spectral, for instance) generate "wiggles" which are also a warning that finer resolution is needed. Vortex methods do not give such warnings; in most applications the vortices look disordered, but the calculation never blows up. This is partly due to its automatic conservation of some key integral quantities (9, 10, 13, 14). Again, the possibility that the calculation is not accurate on small scales but is accurate on the intermediate and large scales is likely.

The most prominent result of a bluff-body calculation is the average drag coefficient C_D. We treated four shapes with sharp corners, so that the primary separation points were fixed, and compared with experimental results (Spalart, 1984, and unpublished). The shapes were a square, an equilateral triangle in two positions and a vertical flat plate or thin airfoil. They were all treated with the same code and roughly the same resolution (typically 1000 vortices). The results are summarized in a table (the $\rightarrow$ indicates the

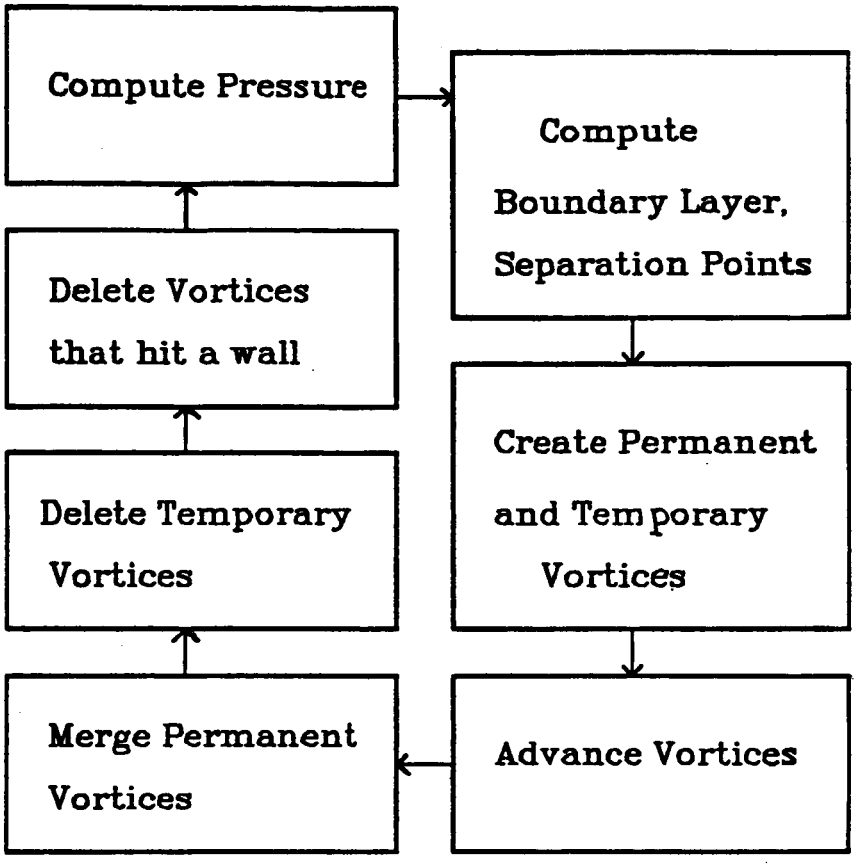

Figure 12. Flow chart of the KPD2 code

direction of the freestream velocity).

Shape	C_D(calc.)	C_D(exp.)
→ □	1.5	2.
→ ▷	2.9	2.
→ ◁	2.4	1.3
→ |	2.8	1.75

The uncertainty is at least ± 0.2 on all the values. Even then, the disagreements are significant. Note also that the calculation often over-predicts C_D, but not always. In general, the shedding frequency (Strouhal number) is better predicted than the drag. These results are not very satisfactory, but we were unable to improve them or to convincingly demonstrate the convergence of the method, even via large variations of the numerical parameters (N, Δt, d_0, etc.). The above table provides a severe but conservative estimate of the performance of the author's method. In some cases, the agreement with experiment is much better, within 5% (see §*10.1*).

Many of the comparable methods also overpredict the drag. One reaction to this is to introduce a "fudge factor" to bring the drag down. Arguing that cancellation of vorticity of opposite signs occurs in reality but not in the calculation (which is not even obvious) some authors arbitrarily make the circulation of the vortices decay as they move into the wake. By adjusting the decay rate one can get any drag one wants. In the author's mind the idea of invoking Kelvin's theorem, building a method around it, and then violating it just to fine-tune one global quantity, C_D, is strange.

Milinazzo and Saffman (1977) already pointed out that "comparison with gross experimental features, such as drag, is not conclusive, and in any case the real flows are turbulent, and therefore three-dimensional, at large Reynolds numbers." This point is valid, especially if the experimental flow has large-scale three-dimensionality. It is possible that much of the drag difference is due to this effect. The author's calculation of dynamic stall (figure 7) agreed with experiment better than those for steady bodies. In this case, the whole span of the wing oscillates in phase, which makes the flow more two-dimensional. The degree of three-dimensionality of the flow past 2-D shapes, such as a circular cylinder or a backward-facing step, is a matter of debate and the subject of ongoing experiments. Reliable numerical simulations should also be obtained in the next few years.

In summary, there is no recipe for the estimation of the errors in a vortex calculation of a complex flow like figure 1. It is essential to monitor the vortices and velocity field as in figure 1 or 4b, but this is only as good as the user's intuition of what the flow should look like. Finally, it should be remembered that we are looking at very challenging flows. If one tackled the multi-element airfoil with an existing finite-difference method, very probably the best one could do is a rather crude calculation which would not enter its convergence pattern, at least not with a reasonable number of points. One would also be dependent on crude transition and turbulence models similar to those we used, so that the viscous effects are very delicate with any method. When applied to complex flows, the vortex method will not yield perfect results, but it will yield very useful ones.

10. TREATMENT OF CASCADES AND SCREENS

10.1. Spatially-Periodic Flows

The computation of 2-D flows that are spatially periodic in one direction is almost as simple as that of unbounded flows, and is useful for the treatment of temporally-developing mixing layers and of cascades, for instance. Complex notation is convenient here. Lamb (1945, p. 224) gives the formula for the stream function generated by a row of vortices of circulation Γ at the points $z_0 + np$, n being any integer (z_0 and p are complex):

$$\psi(z) = \frac{\Gamma}{2\pi} \log\left[\left|\sin\left(\frac{\pi(z - z_0)}{p}\right)\right|\right]. \tag{52}$$

Compare this formula with (8). This function can be regularized by a "core" as in unbounded flows and a convenient one is the analog of (46):

$$\psi_\sigma(z) = \frac{\Gamma}{4\pi} \log\left[\left|\frac{p}{\pi} \sin\left(\frac{\pi(z - z_0)}{p}\right)\right|^2 + \sigma^2\right]. \tag{53}$$

The rest of the method is identical to the unbounded case; one simply substitutes (53), for the stream function, and its derivatives, for the velocity. See §*9.4* for a tip in programming (53). To make the visualizations consistent one chooses a "main period" between some value z_1 and $z_1 + p$; if a vortex moves out of the main period (i.e., if the real part of $(z - z_1)/p$ leaves the interval $[0, 1]$) the vortex is translated by $\pm p$ so that all the vortices can be seen next to each other.

An example of a periodic calculation is the study of a row of chevrons, shown in figure 13. These chevrons were candidates for an acoustic barrier around the inlet of a wind tunnel at NASA Ames Research Center. The pressure drop across the barrier was estimated to be of the order of 5 to 10 times the dynamic pressure, based on the ratio of the open area to the pitch of the cascade (essentially the argument of Batchelor, 1967, p. 375). The calculation predicted a much larger value: 86 times the dynamic pressure. The issue was settled when experiments by Professor J. Foss (Michigan State University) produced a value of 82. Such losses were unacceptable, and the design was dropped. The open-area argument vastly underestimated the loss of energy in the flow due to the repeated separations. This was one of the more successful and directly useful applications of the method.

*10.2. A Simple Model for Screens**

Screens are often used in wind tunnels to generate homogeneous turbulence, to introduce a pressure drop (e.g., for mixing-layer studies), or sometimes to smooth out an irregular flow and prevent separation on a cascade. Here we present a simple, *macroscopic* model that can account for the latter three effects and is a good exercise in itself. It was used in the chevron calculations (see figure 13). It could be used for nonperiodic geometries too.

Consider for simplicity a screen along the y axis in 2-D. We model it as a pressure jump $\Delta p(y) \equiv p(0^+, y) - p(0^-, y)$. The effect of the screen on the fluid is equivalent to a body

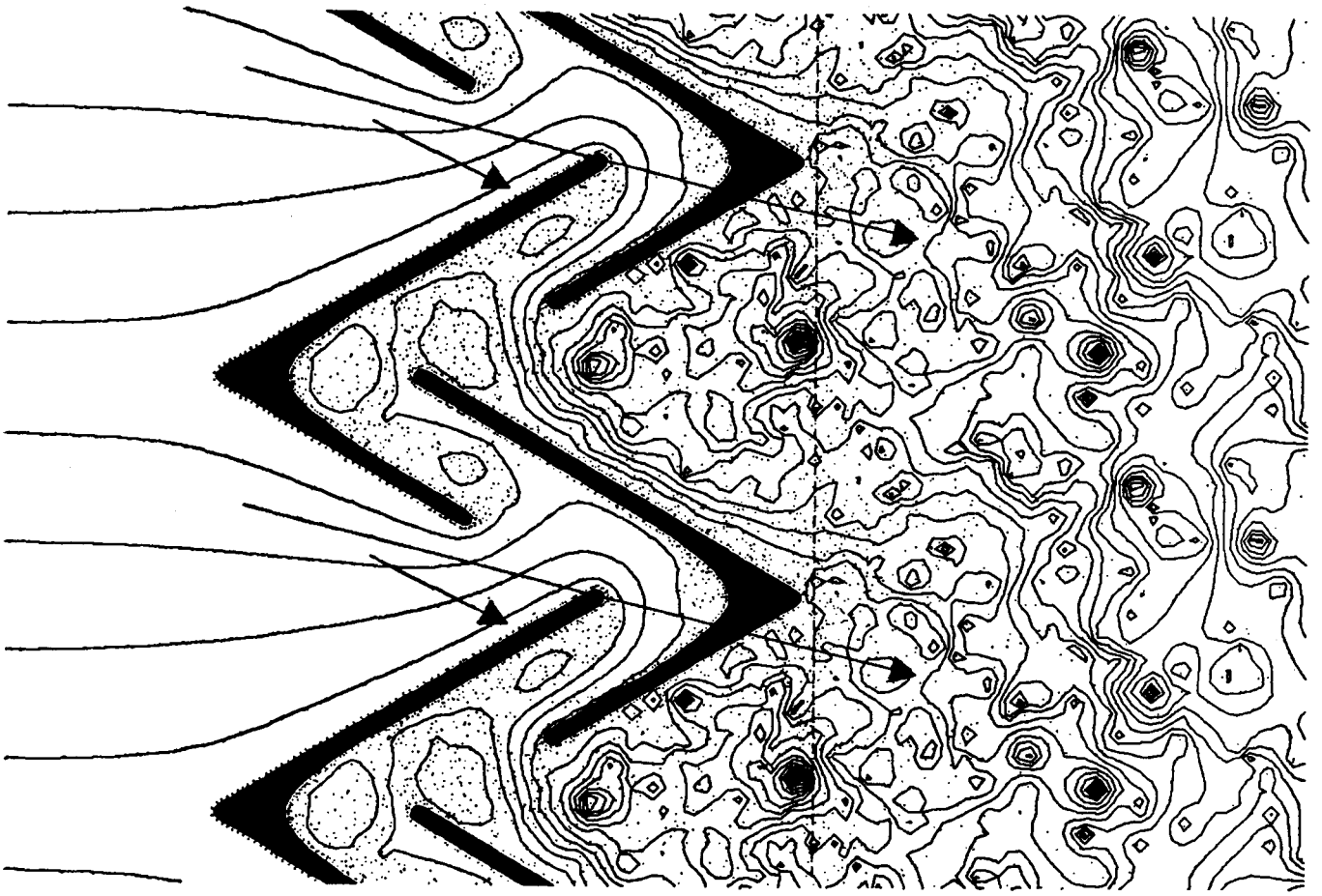

Figure 13. Flow past two rows of chevrons. $\cdots$ vortices; $\longrightarrow$ forces; — streamlines; - - - screen

force $\mathbf{f} = \Delta p(y)\delta(x)\mathbf{e_x}$ with δ the 1-D Dirac distribution and $\mathbf{e_x}$ the unit vector in x. To obtain the effect on the vorticity we take the curl of $\mathbf{f}$ which is $-d(\Delta p)/dy\ \delta(x)$. There is a generation of vorticity at the rate $-d(\Delta p)/dy$ per unit length in y and unit time. This is easily modeled by creating new vortices along the screen at each time step.

We still have to prescribe the value of Δp. In the chevron calculations a pressure drop proportional to the local dynamic pressure was assumed, that is: $\Delta p = -C\ u|u|/2$ where u is the local velocity in the x direction and C is a positive constant and in general depends on the solidity of the screen, the shape of the bars, and so on. C was set to 2. Near the center of figure 13 there is a jet (closely spaced streamlines, corresponding to high velocity); notice how it spreads out when it encounters the resistance of the screen, as expected, resulting in a slightly more uniform flow behind the screen.

So far, the simplest method has been used for the time integration: the value of u at one step is used to compute Δp and the circulation of the new vortices for the next step. This method worked with the parameters used in the chevron study, but will produce an instability for large enough values of the product $C|u|\Delta t/\Delta y$, where Δy is the spacing of

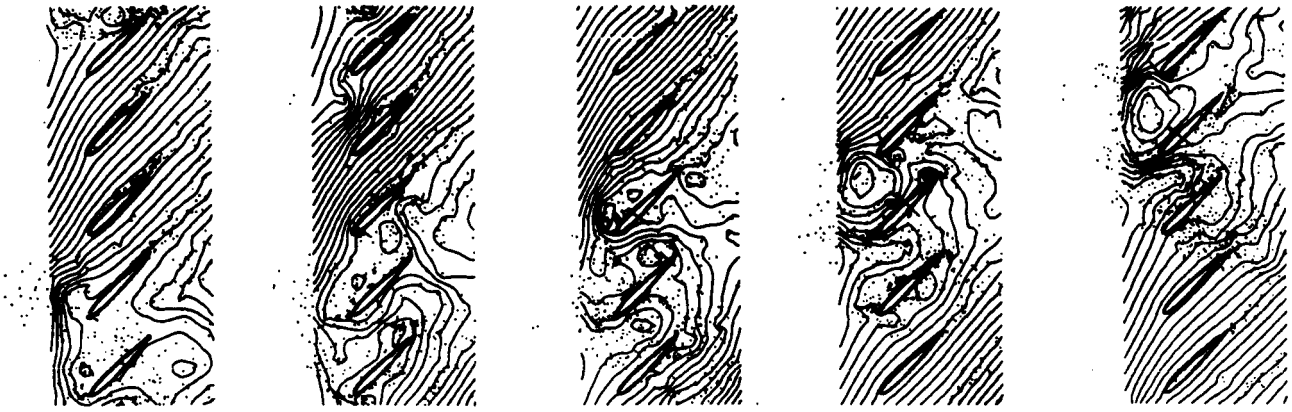

Figure 14. Propagation of a stall cell in a cascade. ··· vortices; ↑ forces; — streamlines

the points that describe the screen. For large values of the product (in the limit $C \to \infty$ one actually has a solid wall) one will need a fully coupled algorithm, instead of one which goes back and forth between the fluid and the screen.

*10.3. Computation of Rotating Stall in a Cascade**

The periodic version of the method was also applied to 2-D cascades of airfoils with the hope of observing "rotating stall", or more appropriately "traveling stall" (since the cascade is actually not circular). When a compressor stalls, the stall pattern is often uneven from blade to blade, and stall cells tend to propagate around the compressor at a fraction of the velocity of the blades. Such a flow involves a multiply-connected domain (since several blades are involved) and large regions of separation, which makes it a good candidate for the vortex method.

Figure 14 is taken from Spalart (1984, 1985). Five NACA 0012 airfoils are included within the numerical period p. They are at 45° to the plane of the cascade. The incoming flow, of magnitude U_0, gives them a 30° incidence. Let c denote the chord of the airfoils; the pitch was chosen equal to c. The time interval between frames in the figure is $2c/U_0$. The computation was started from irrotational flow with a dipole in the wake (to break the blade-to-blade periodicity) and has been running long enough to reach a well-developed state (see Spalart, 1985, for the transient behavior and other values for the stagger and inflow angles). One observes a stall cell which alters the flow near two of the blades, and drastically reduces or even reverses the mass flux between them. The cell propagates upwards at about 40% of U_0. This figure, and the flow pattern, are in qualitative agreement with flow visualizations, but more detailed comparisons were not attempted. The method is limited by its reliance on rather crude transition and turbulence models (as in the dynamic-stall study), by the resolution which is becoming marginal (100 wall points and 300 vortices per blade), and by the fact that it is 2-D. However Speziale, Sisto, and Jonnavithula (1986) extended the study to cambered airfoils and a wider parameter range.

11. TIME-SAVING ALGORITHMS*

*11.1. Vortex-in-Cell Methods**

These methods discard the Green's-function approach (3, 6, 8) and solve the Poisson equation for the stream function by a grid method (Christiansen, 1973). Typically, with N' grid points the solution is obtained in $O(N' \log(N'))$ operations, so if N' is comparable with N the vortex-in-cell method is much faster than the $O(N^2)$ method. In practice N' is at least as large as N, and could be much larger if the vorticity distribution is very intermittent. The procedure is to define a grid and to obtain vorticity values at the grid points according to the circulation of the vortices (if any) present in the adjoining cells. The vorticity is "transferred" to the grid, but only for the Poisson solution; the vortices retain their identity. The beauty of this method is that it still has the low-dispersion advantage of other vortex methods. Once the stream function is available it is differentiated to obtain the grid values of the velocity. The velocity is then interpolated to the position of the vortices and the vortices are moved, thus completing the work for this time step.

The best applications are those in which N' can be kept to a value close to N, that is, when the vortical region is rather predictable and of simple shape, for instance an internal flow or a mixing layer (Aref and Siggia, 1980, Couët, Buneman, and Leonard, 1981). In such cases, one can save a large fraction of the computational effort. The method is not grid-free, and since boundary conditions are needed on ψ the grid has to be body-fitted. This would be a serious drawback in engineering applications. Note also that the transfer and interpolation steps have a cost only $O(N)$, but are hardly vectorizable. Another topic of research is in the local errors associated with the exchange of information between the regularly-arranged grid points and the vortices, which can fall in any region of the grid cell. The grid destroys the isotropy of the algorithm, and in general a vortex will have a spurious self-induced velocity. See the work by Couët *et al.* (1981) and Anderson (1985b).

*11.2. Lumping Methods**

These methods still use the Biot-Savart approach, but reduce the operation count by approximating some of the interaction terms in (26), using Taylor expansions. Spalart and Leonard (1981) presented such an algorithm, claiming an operation count of order $N^{3/2}$. L. Greengard and Rokhlin (1987) claim $O(N)$ for their algorithm. Divide the domain where the vortices are into a regular array of cells. The cells are of size l, large enough to contain many vortices each (in contrast with the vortex-in-cell method). They can overlap with the solid body; in that sense the method is "practically" grid-free since the grid is not body-fitted. Now consider two cells that are separated by at least a few times l. The interactions are proportional to $1/z$, using complex notation. This function is analytic and has a rapidly converging Taylor expansion. If Z_L and Z_K are the cell centers, z_i is in cell L, and z_j in cell K, we Taylor-expand the function $1/z$ in the vicinity of $Z_K - Z_L$; see figure 15.

There are several options. The requirement is to incur a relative error of less than some small number ϵ on any of the terms. Spalart and Leonard chose to use a varying number

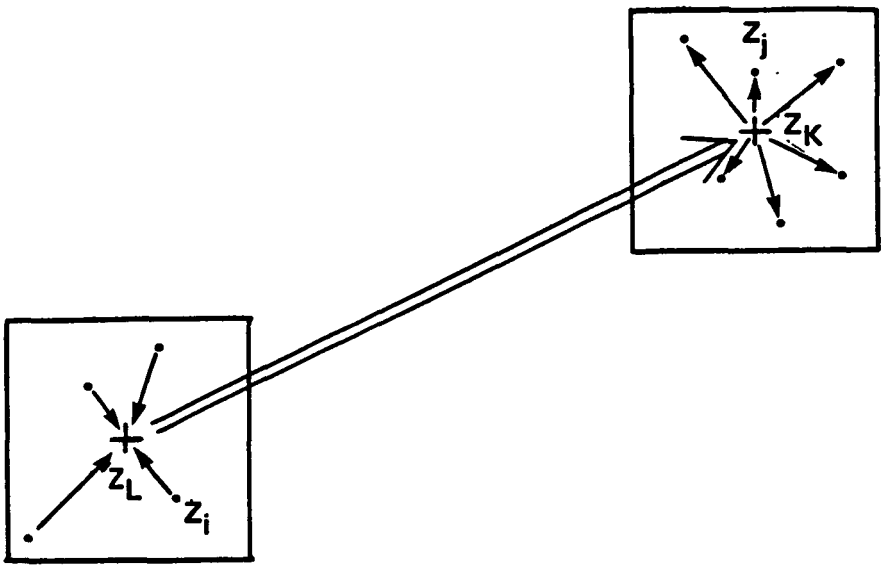

Figure 15. Schematic of cell-to-cell interactions in the "lumping" methods

of terms depending on the value of $|Z_K - Z_L|/l$ (more terms if it is small). If the cells are neighbors the interactions are computed vortex-by-vortex, because the Taylor expansion fails (i.e., it is too close to its radius of convergence). One can optimize the number of cells, and the best value is of order $N^{1/2}$. The overall cost, for a fixed value of ϵ, is then of order $N^{3/2}$. Greengard and Rokhlin (1987) carry the idea further by nesting the cells. There are many levels of lumping. In essence they keep $|Z_K - Z_L|/l$ roughly constant, instead of varying the number of terms. Spalart and Leonard (1981) wasted terms on the very-well separated cells (large $|Z_K - Z_L|/l$). The nesting removes the need for computing many vortex-by-vortex terms. On the other hand, one needs many more cells. Greengard and Rokhlin's arrive at an operation count of order $N \log^2(\epsilon)$.

Greengard and Rokhlin's (1987) statement that the cost is of order N is not rigorously correct, because ϵ is not a constant (there is no reason why it should equal the precision of the computer). For the method to converge, ϵ must tend to zero like some power of N as N tends to ∞. Thus the cost is really of order $N \log^2(N)$. Similarly, Spalart and Leonard's $N^{3/2}$ estimate should be revised upwards, at least to $N^{3/2} \log(N)$, because as $\epsilon \rightarrow 0$ one needs to include more Taylor terms for a given separation. A factor $\log(N)$ is not very important especially since larger values of N improve the throughput of the computer, but one likes to be rigorous if possible.

In practice, Spalart and Leonard's (1981) algorithm was helpful on serial computers (CDC 7600) with $\epsilon = 10^{-2}$, but was hardly worth the effort on vector computers (Cray 1S), because it makes vectorization difficult and results in short loops. One probably needs thousands of vortices for the lumping to bring a significant improvement (the gather-scatter capabilities of the newest machines may make a difference). Greengard and Rokhlin report

an impressive advantage starting with a few hundred vortices and with $\epsilon \approx 10^{-5}$, again on a serial machine (a VAX 8600). The performance of their method on a vector machine will be extremely interesting. The nested method is very promising, and the fact the grid does not interfere with the body is a definite advantage over vortex-in-cell methods. Also, empty cells do not consume any work. The extension to 3-D will require more work since we are not just considering the function $1/z$, but is possible.

REFERENCES

ANDERSON, C. 1985a A vortex method for flows with slight density variations. *J. Comp. Phys.* **61,** 417.

ANDERSON, C. 1985b A method of local corrections for computing the velocity field due to a distribution of vortex blobs. *J. Comp. Phys.* **62,** 111.

ANDERSON, C. AND GREENGARD, C. 1985 On vortex methods. *SIAM J. Num. Anal.* **22,** 413.

AREF, H. 1983 Integrable, chaotic, and turbulent vortex motion in two-dimensional flows. *Ann. Rev. Fluid Mech.* **15,** 345.

AREF, H. AND SIGGIA, E. D. 1980 Vortex dynamics of the two-dimensional turbulent shear layer. *J. Fluid Mech.* **100, 4,** 705.

ASHURST, W. T. 1979 Numerical simulation of turbulent mixing layers via vortex dynamics. Turbulent Shear Flows I; F. Durst, B. E. Launder, F. W. Schmidt and J. H. Whitelaw editors. Springer-Verlag, Berlin, 1979.

ASHURST, W. T. 1983 Large-eddy simulation via vortex dynamics. *A. I. A. A.* **83-1879-CP.**

ASHURST, W. T. AND MEIBURG, E. 1985 Three-dimensional shear layers via vortex dynamics. SANDIA Report 85-8777. Also to appear in *J. Fluid Mech.*

BATCHELOR, G. K. 1967 An introduction to fluid dynamics. Cambridge Univ. Press.

BEALE J. T. AND MAJDA, A. 1982 Vortex methods, I and II. *Math. Comp.* **39,** 1.

BEALE J. T. AND MAJDA, A. 1985 High-order accurate vortex methods with explicit velocity kernels. *J. Comp. Phys.* **58,** 188.

BIRKHOFF, G. 1962 Helmholtz and Taylor instability. *Proc. Symp. Appl. Math., Amer. Math. Soc.* **XIII,** 55.

CANTALOUBE, B. AND HUBERSON, S. 1984 A vortex point method for calculating inviscid incompressible flows around rotary wings. *Rech. Aérosp.* **1984-6,** 19.

CEBECI, T. AND BRADSHAW, P. 1977 Momentum transfer in boundary layers. McGraw-Hill, New York.

CHEER, A. Y. 1983 Numerical study of incompressible slightly viscous flow past blunt bodies and airfoils. *SIAM J. Sci. Stat. Comp.* **4, 4,** 685.

CHORIN, A. J. 1973 Numerical study of slightly viscous flow. *J. Fluid Mech.* **57,** 785.

CHORIN, A. J. 1978 Vortex-sheet approximation of boundary layers. *J. Comp. Phys.* **27,** 428.

CHORIN, A. J. 1980 Vortex models and boundary-layer instability. *SIAM J. Sci. Stat. Comp.* **1, 1,** 1.

CHORIN, A. J. 1982 The evolution of a turbulent vortex. *Commun. Math. Phys.* **83,** 517.

CHORIN, A. J. AND BERNARD, P. S. 1973 Discretization of a vortex sheet, with an example of roll-up. *J. Comp. Phys.* **13,** 423.

CHRISTIANSEN, J. P. 1973 Numerical simulation of hydrodynamics by the method of point vortices. *J. Comp. Phys.* **13,** 363.

COUËT, B., BUNEMAN, O. AND LEONARD, A. 1981 Simulation of three-dimensional incompressible flows with a vortex-in-cell method. *J. Comp. Phys.* **39,** 305.

DEFFENBAUGH, F. D. AND MARSHALL, F. J. 1976 Time development of the flow about an impulsively started cylinder. *A. I. A. A. J.* **14,** 908.

DEFFENBAUGH, F. D. AND SHIVANANDA, T. P. 1980 Discrete vortex wake modeling of separated flow phenomena. TRW Report 33945-UT-00, Redondo Beach, Calif.

GHONIEM, A. F. AND GAGNON, Y. 1987 Vortex simulation of laminar recirculating flow. *J. Comp. Phys.* **68,** 346.

GOODMAN, J. 1987 Convergence of the random vortex method. *Comm. Pure Appl. Math..* **XL,** 189.

GREENGARD, C. A. 1984 Three-dimensional vortex methods. Ph. D. Thesis, Lawrence Berkeley Lab. Rep. 18217.

GREENGARD, C. A. 1985 The core-spreading vortex method approximates the wrong equation. *J. Comp. Phys.* **61,** 345.

GREENGARD, C. A. AND THOMANN, E. 1988 Point vortices, vortons, and weak solutions of the Euler equations. submitted to *Phys. Fluids.*

GREENGARD, L. AND ROKHLIN, V. 1987 A fast algorithm for particle simulations. *J. Comp. Phys.* **73,** 325.

HALD, O. 1979 The convergence of vortex methods, II. *SIAM J. Num. Anal.* **16,** 726.

HALD, O. 1984 Convergence of a random method with creation of vorticity. Center for Pure App. Math., PAM-252, U. C. Berkeley .

HAMA, F. R. 1962 Progressive deformation of a perturbed line-vortex filament. *Phys. Fluids.* **6,** 526.

HASIMOTO, H. 1972 A soliton on a vortex filament. *J. Fluid Mech.* **51,** 477.

KATZ, J. 1981 A discrete vortex method for the non-steady separated flow over an airfoil. *J. Fluid Mech.* **102,** 315.

KRASNY, R. 1986 A study of singularity formation in a vortex sheet by the point-vortex approximation. *J. Fluid Mech.* **167,** 65.

LAMB, H. 1945 Hydrodynamics. Dover, New York.

KUWAHARA, K. AND TAKAMI, H. 1973 Numerical studies of two-dimensional vortex motion by a system of point vortices. *J. Phys. Soc. Japan.* **34,** 247.

LEONARD, A. 1980 Vortex methods for flow simulation. *J. Comp. Phys.* **37,** 289.

LEONARD, A. 1985 Computing three-dimensional incompressible flows with vortex elements. *Ann. Rev. Fluid Mech.* **17,** 523.

LEWIS, R. I. 1981 Surface vorticity modelling of separated flows from two-dimensional bluff bodies of arbitrary shape. *J. Mech. Eng. Sci.* **23, 1,** 1.

LIGHTHILL, M. J. 1963 Boundary-layer theory. in Laminar Boundary Layers, ed. by L. Rosenhead. Oxford Univ. Press.

MARCHIORO, C. AND PULVIRENTI, M. 1983 Euler evolution for singular initial data and vortex theory. *Comm. Math. Phys.* **91,** 563.

MELANDER, M. V., ZABUSKY, N. J., AND STYCZEK, A. S. 1986 A moment model for vortex interactions of the two-dimensional Euler equations. Part 1. Computational validation of a Hamiltonian elliptical representation. *J. Fluid Mech.* **167,** 95.

MILINAZZO, F., AND SAFFMAN, P. G. 1977 The calculation of large-Reynolds-number two-dimensional flow using discrete vortices with random walk. *J. Comp. Phys.* **23,** 380. See also **26,** 453.

MOORE, D. W. 1979 A numerical study of the roll-up of a finite vortex sheet. *J. Fluid Mech.* **63,** 225.

MOSHER, C. 1985 A method for computing three-dimensional vortex flows. *Zeit. Flugwiss. Weltraumforsch.* **9, 3,** 125.

NAKAMURA, Y., LEONARD, A., AND SPALART, P. R. 1982 Vortex simulation of an inviscid shear layer. *A. I. A. A.* **82-0948.**

NAKAMURA, Y., LEONARD, A., AND SPALART, P. R. 1986 Internal structure of a vortex breakdown. *A. I. A. A.* **86-1074.**

NOVIKOV, E. A. 1983 Generalized dynamics of three-dimensional vortical singularities (vortons). *Sov. Phys. JETP.* **57, 3,** 566.

PERLMAN, M. B. 1985 On the accuracy of vortex methods. *J. Comp. Phys.* **59,** 200.

PRANDTL, L. AND TEITJENS, O. G. 1934 Applied Hydro- and Aeromechanics. Dover, New York.

REHBACH, C. 1977 Calcul numérique d'écoulements tridimensionnels instationnaires avec nappes tourbillonaires. *Rech. Aérosp.* **1977-5,** 289. Also *A. I. A. A.* **78-111.**

ROBERTS, S. 1985 Accuracy of the random vortex method for a problem with nonsmooth initial conditions. *J. Comp. Phys.* **58,** 29.

ROSENHEAD, L. 1931 The formation of vortices from a surface of discontinuity. *Roy. Soc. London.* **A 134,** 170.

SAFFMAN, P. G. 1980 Vortex interactions and coherent structures in turbulence, in Transition and turbulence, R. E. Meyer editor. Academic, New York.

SAFFMAN, P. G. AND MEIRON, D. I. 1986 Difficulties with three-dimensional weak solutions for inviscid incompressible flow. *Phys. Fluids.* **29, 8,** 2373.

SPALART, P. R. 1984 Two recent extensions of the vortex method. *A. I. A. A.* **84-0343.**

SPALART, P. R. 1985 Simulation of rotating stall by the vortex method. *J. Propulsion Power.* **1, 3,** 235.

SPALART, P. R. AND LEONARD, A. 1981 Computation of separated flows by a vortex-tracing algorithm. *A. I. A. A.* **81-1246.**

SPALART, P. R., LEONARD, A., AND BAGANOFF, D. 1983 Numerical simulation of separated flows. NASA T. M. 84328.

SPEZIALE, C. G., SISTO, F. AND JONNAVITHULA, S. 1986 Vortex simulation of propagating stall in a linear cascade of airfoils.. *J. Fluids Eng.* **108,** 304.

STANSBY, P. K. AND DIXON, A. G. 1982 The importance of secondary shedding in two-dimensional wake formation at very high Reynolds numbers. *Aero. Quart.* **33, 2,** 105.

TENG, Z. H. 1982 Elliptic-vortex method for incompressible flow at high Reynolds number. *J. Comp. Phys.* **46,** 54.

TING, L. 1983 On the application of the integral invariants and decay laws of vorticity distributions. *J. Fluid Mech.* **127,** 497.

WINCKELMANS, G. AND LEONARD, A. 1987 Short wave-length dynamics of a vortex filament. *Bull. Amer. Phys. Soc.* **32, 10,** 2078.

WU, J. C., AND SANKAR, N. L. 1980 Aerodynamic force and moment in steady and time-dependent viscous flows. *A. I. A. A.* **80-0011. See also** *A. I. A. A. J.* **19, 4, 432.**

ZABUSKY, N. J., HUGHES, M. H., AND ROBERTS, K. V. 1979 Contour dynamics for the Euler equations in two dimensions. *J. Comp. Phys.* **30,** 96.

NASA
National Aeronautics and Space Administration

Report Documentation Page

1. Report No.	2. Government Accession No.	3. Recipient's Catalog No.
NASA TM-100068		

4. Title and Subtitle	5. Report Date
Vortex Methods for Separated Flows	June 1988
	6. Performing Organization Code

7. Author(s)	8. Performing Organization Report No.
Philippe R. Spalart	A-88097
	10. Work Unit No.
	505-60

9. Performing Organization Name and Address	11. Contract or Grant No.
Ames Research Center Moffett Field, CA 94035	
	13. Type of Report and Period Covered
12. Sponsoring Agency Name and Address	Technical Memorandum
National Aeronautics and Space Administration Washington, DC 20546-0001	14. Sponsoring Agency Code

15. Supplementary Notes

Point of Contact: Philippe R. Spalart, MS 202A-1, Ames Research Center, Moffett Field, CA 94035
(415) 694-4734 or FTS 464-4734

16. Abstract

The numerical solution of the Euler or Navier-Stokes equations by Lagrangian "vortex methods" is discussed. The mathematical background is presented in an elementary fashion and includes the relationship with traditional point-vortex studies, the convergence to smooth solutions of the Euler equations, and the essential differences between two- and three-dimensional cases. The difficulties in extending the method to viscous or compressible flows are explained.

The overlap with the excellent review articles available is kept to a minimum and more emphasis is placed on the author's area of expertise, namely two-dimensional flows around bluff bodies. When solid walls are present, complete mathematical results are not available and one must adopt a more heuristic attitude. The imposition of inviscid and viscous boundary conditions without conformal mappings or image vortices and the creation of vorticity along solid walls are examined in detail. Methods for boundary-layer treatment and the question of the Kutta condition are discussed.

Practical aspects and tips helpful in creating a method that really works are explained. The topics include the robustness of the method and the assessment of accuracy, vortex-core profiles, timemarching schemes, numerical dissipation, and efficient programming. Operation counts for unbounded and periodic flows are given, and two algorithms designed to speed up the calculations are described.

Calculations of flows past streamlined or bluff bodies are used as examples when appropriate. These include curved mixing layers, the starting vortex and the dynamic stall of an airfoil, rotating stall in a two-dimensional cascade, a multi-element airfoil, and an attempt at predicting the drag crisis of a circular cylinder.

17. Key Words (Suggested by Author(s))	18. Distribution Statement
Numerical simulation Discrete vortices Separated flows	Unclassified – Unlimited Subject Category – 02

19. Security Classif. (of this report)	20. Security Classif. (of this page)	21. No. of pages	22. Price
Unclassified	Unclassified	73	A05